行政院國家科學委員會專題研究計畫　成果報告

前瞻性發光元件應用之寬能隙氮化合物材料研究(2/2)

計畫類別：個別型計畫
計畫編號：NSC92-2215-E-002-010-
執行期間：92 年 08 月 01 日至 93 年 10 月 31 日
執行單位：國立臺灣大學光電工程學研究所

計畫主持人：楊志忠

計畫參與人員：Chih-Chung (C. C.) Yang, Art&#363；ras &#381；ukauskas and Ivars T&#257；le

報告類型：完整報告
報告附件：國際合作計畫研究心得報告
處理方式：本計畫可公開查詢

中　華　民　國 94 年 4 月 7 日

PROGRAM ON MUTUAL FUNDS FOR THE SCIENTIFIC CO-OPERATION OF REPUBLIC OF LITHUANIA AND REPUBLIC OF LATVIA WITH REPUBLIC OF CHINA (TAIWAN)

REPORT

on

MATERIALS RESEARCH ON WIDE BAND GAP GROUP III NITRIDE COMPOUNDS FOR ADVANCED LIGHT EMITTERS

SECOND YEAR (2003-2004)

Submitted to: National Science Council, Bonn office, Bonn, Germany

National Science Council, Taipei, Taiwan, Republic of China

Department of Science and Higher Education under the Ministry of Education and Science, Vilnius, Lithuania

Department of Higher Education & Science of the Ministry of Education and Science, Riga, Latvia

Submitted by: Prof. Dr. Chih-Chung (C. C.) Yang
Graduate Institute of Electro-Optical Engineering, National Taiwan University,
1, Roosevelt Road, Sec. 4, Taipei, Taiwan, Republic of China
Tel: 886 2 23657624, Fax: 886 2 23652637, E-mail: ccy@cc.ee.ntu.edu.tw

Prof. Habil. Dr. Artūras Žukauskas
Institute of Materials Science and Applied Research, Vilnius University,
Sauletekio al. 9, building III, LT-10222 Vilnius, Lithuania
Tel/Fax: 3705 2 366059, E-mail: arturas.zukauskas@ff.vu.lt

Prof. Dr. Habil. Phys. Ivars Tāle
Institute of Solid State Physics, University of Latvia,
8 Kengaraga Str. LV-1063 Riga, Latvia
Tel: 371 7 260639, Fax: 371 7 112583, E-mail: iatale@latnet.lv

April 2004

MATERIALS RESEARCH ON WIDE BAND GAP GROUP III NITRIDE COMPOUNDS FOR ADVANCED LIGHT EMITTERS
SECOND YEAR (2003-2004)

CONTENS

MATERIALS RESEARCH ON WIDE BAND GAP GROUP III NITRIDE COMPOUNDS FOR ADVANCED LIGHT EMITTERS
SECOND YEAR (2003-2004)

Resume

The joint Lithuanian-Latvian-Taiwanese project on "MATERIALS RESEARCH ON WIDE BAND GAP GROUP III NITRIDE COMPOUNDS FOR ADVANCED LIGHT EMITTERS" addresses materials quality issues of group III nitride semiconductors. A wide-range of optical spectroscopy experiments and theoretical modeling applied enabled us to perform materials characterization in InGaN/GaN quantum well structures used for green-blue light emitting diode and semiconductor laser applications.

During the second year of the project, InGaN/GaN quantum well structures with various well width and indium content, prepared by Taiwan side, were characterized by traditional optical spectroscopy and high-resolution microscopy including strain state analysis. Further, samples were studied by Lithuanian and Latvian groups by applying complementary methods of materials characterization based on photoluminescence, photoluminescence excitation, time-resolved photoluminescence, photoluminescence power excitation, photoreflectance, and modeling by conventional Schroedinger-Poison, Monte Carlo and *ab-initio* approches.

Combined materials postgrowth characterization enabled us to give recommendations on InGaN/GaN multiple quantum well thermal treatment. The performed optical and microstructure analysis evidences on an improvement of the MQW structural quality and increased emission efficiency in thicker structures upon post growth thermal annealing. Combined experiments on spontaneous and stimulated emission performed at high intensity excitation together with analysis of the excitation power dependences of luminescence enabled us to estimate increased variation of the random band potential with increasing the well width. Differences in degree of disorder in as-grown samples of various well width were shown to lead to different impact of thermal annealing on luminescence from localized states. The results are accounted for in terms of annealing-invoked In–Ga interdiffusion, which behaves as either diffusion of indium to barriers or "up-hill" diffusion within the wells depending on the well width.

Temperature dependence of the photoluminescence linewidth in thin InGaN/GaN multiple quantum wells was analyzed using Monte Carlo simulation of exciton hopping. The dependence was shown to reveal a crossover from nonthermalized to thermalized exciton energy distribution at about 150 K and fluctuations of the band potential with additional broadening that was attributed to formation of In-rich regions. Based on the fitting procedure, band potential fluctuations within In-rich regions (31 meV) and dispersion of the average exciton energy in different In-rich regions (29 meV) were extracted. The localized-state energy dispersion for hopping of excitons within isolated In-rich regions increase with increasing In content from 31 meV in the sample with the lowest In content to 38 meV in sample with the highest In content. Meanwhile, the dispersion due to different average indium content within the In-rich regions changes from 29 to 47 meV in the same samples, respectively. A Bose-Einstein-like temperature dependence of the exciton energy in the wells was reconstructed and proved by photoreflectance measurements of the mean exciton energy.

The deep level transient spectroscopy (DLTS) for investigation of trapping states in GaN muli quantum well structures has been installed and approved. In order to assess the usability of DLTS technique for study the deep trapping levels in multi-quantum well

structures both the thermostimulated depolarization (TSD), thermostimulated capacitance relaxation (TSC) and DLTS are studied in p-n homojunction GaN blue diode. The TSD and TSC curves shows that cooling of the GaInN structure down to liquid helium temperatures results in complete trapping both the majority and the minority charge carriers at the shallow dopand levels. Thermal ionization of the dopand states occurs in the temperature region 40 – 60 K. According to the DLTS data the electron level at E_c-E_t=0.3 eV is observed.

Ab initio calculations of the neutral and charged defects in GaN has been provided. The generalized gradient approximation of a density functional theory in LCAO approximation is used to determine electronic structures and formation energies of defects in hexagonal GaN. Formation of localized electronic states followed by localization of excess charge carriers has been considered. Impurities of Mg, Zn, Li, Si and C atoms (the most common dopants) and vacancies of Ga and N are examined. Defects are tested for being centers of an electron localization, therefore calculations of all relevant charged states are done. All calculations are performed for a supercell containing 96 atoms which seems to be enough to neglect defect interaction to its image. Typical atomic relaxations for two nearest neightbours are found to be 4 -5% of the corresponding bond length in a perfect crystal for both impurities and vacancies. Mulliken atomic charge differences are much greater at two nearest neighbours of defect than anywhere else in a crystal. These results imply that such point defects in GaN significantly affect a geometry of only first two coordination spheres.

During the second year, problems of improvement of device performance by Si doping have been addressed. Further study of exciton migration processes together with advanced spectroscopy experiments is foreseen for the next year of the project. Basing on success in understanding of exciton localization and migration processes we believe that performed joint actions on advanced microscopy, optical spectroscopy, and theoretical modeling will enable us to make an significant progress in *quantitative* characterization of device prototype InGaN/GaN systems.

MATERIALS RESEARCH ON WIDE BAND GAP GROUP III NITRIDE COMPOUNDS FOR ADVANCED LIGHT EMITTERS

SECOND YEAR (2003-2004)

I. General part

1.1 Introduction

New generation of semiconductor materials based on group III-V compounds tremendously expands application areas of direct bandgap semiconductors. In particular, group-III nitrides are subject of a huge interest that is classified as "the blue-UV revolution" in optoelectronics.

The joint Lithuanian-Latvian-Taiwanese project on "MATERIALS RESEARCH ON WIDE BAND GAP GROUP III NITRIDE COMPOUNDS FOR ADVANCED LIGHT EMITTERS" addresses materials quality issues of group-III nitride semiconductors that might improve the competitiveness of each country in the field of production and applications of novel short-wave visible and near-UV light emitters.

The successful fabrication of GaN-based light-emitting devices relies on several novel techniques in the growth and process for the devices. However, application of new generation of ternary (InGaN, AlGaN) and quaternary (InAlGaN) wide-band gap semiconductor materials rise fundamental problems in the control of the materials properties and predictions of device electronic structure. Despite of a significant number of scientific publications that relate to optical properties of group-III nitride based compounds and their nanostructures, fundamental mechanisms responsible for efficient photon emission are not well understood so far. In particular, the role of indium aggregation and phase separation in InGaN system in photon emission efficiency are still quite controversial. Also, the role of the built-in electric field effect on emission properties of light emitting diodes and lasers has been unambiguously not unveiled. On the other hand, further promotion of group-III nitride semiconductors is hindered by insufficient materials quality.

Monitoring of the materials quality as well as of the built-in electric fields in quantum structures is a subject of major efforts undertaken by nitride semiconductor physicists and engineers. A variety of conventional characterization methods, such as high-resolution x-ray diffraction (HRXRD), transmission electron microscopy (TEM), atomic force microscopy (AFM), reflection high-energy electron diffraction (RHEED), photoluminescence (PL), time-resolved luminescence (TRL), photoluminescence excitation (PLE), photoluminescence power excitation (PPE), photo-reflection (PR), are used to a provide a feedback for the fabrication and processing of nitride semiconductor devices.

One of the **main goals** of the present project is to enhance the arsenal of materials characterization methods such as high-photoexcitation photoluminescence and optical gain, nonlinear optical spectroscopy as well as study of localized and defect states in combination with theoretical modeling of carrier/exciton dynamics. The advancing of combined

characterization techniques is expected to promote further improvement of materials quality of AlInGaN semiconductor system.

1.2 Participants:

Taiwan group

Prof. C.C. Yang,
Yi-Yin Chung, Shih-Wei Feng, Yung-Chen Cheng, Chih-Wen Liu, En-Chiang Lin
Department of Electrical Engineering and Graduate Institute of Electro-Optical Engineering, National Taiwan University, Taipei, Taiwan, R.O.C.

Yen-Sheng Lin and Cheng Hsu
Department of Mechanical Engineering, Chung Cheng Institute of Technology, National Defense University, Tahsi, Taoyuan, Taiwan, R.O.C.

Kung-Jen Ma
Department of Mechanical Engineering, Chung Hua University, Hsinchu, Taiwan, R.O.C.

Hui-Wen Chuang, Cheng-Ta Kuo, and Jian-Shihn Tsang
Advanced Epitaxy Technology Inc., Hsinchu Industrial Park, Taiwan, R.O.C.

Latvian group

Prof. I.Tale,

Dr. phys. M. Springis, Dr. phys. P. Kulis, and Dr. phys. U. Rogulis,

Bn. stud. M. Piesins, Bn. stud. I. Gromulis, M.stud. A. Sarkovskis and M.stud. A. Gulans

Institute of Solid State Physics University of Latvia, Riga, Latvia.

Lithuanian group

Prof. A.Žukauskas,

Prof. S.Juršėnas, Prof. G.Tamulaitis, Dr. G.Kurilčik,

Ph.D student S. Miasojedovas, Ph.D student K. Kazlauskas, undergraduate students J. Mickevičius and P. Pobedinskas

Institute of Materials Science and Applied Research, Vilnius University, Vilnius, Lithuania

1.3 Research coordination

Mutual e-mail communications of the group leaders Prof. C. C. Yang, Prof. A. Žukauskas, and Prof. I Tale were employed to coordinate the joint work. Much effort in the second year of the project was paid to integration of experimental abilities and expertise within three groups.

The detailed working plan for the second year was discussed during the visit of Prof . S.Jursenas (Taipei, Taiwan, May 2003). A new set of InGaN/GaN multiple quantum wells varying in In content was selected for detailed spectroscopy experiments and theoretical modeling.

Joint experiments of Latvian and Lithuanian groups were organized by mutual exchange of the samples and visits of Habil Dr. M. Springis to Vilnius (October–November 2003).

Summarization and final exchange of the results of the second year on post-growth optical characterization of the multiple quantum wells has been organized by the visits of Prof. S. Juršėnas to Riga in (March 2004) and to Taipei (April to May 2004).

The further work is expected to be discussed by the group leaders during the International Workshop on Nitride Semiconductors IWN2004, July 19-23, 2004 Pittsburgh, Pennsylvania, USA.

1.4 Brief description of the activities performed in 2003-2004 year

The main direction of research performed by **Taiwan group** in 2003-2004 year was optimization of thermal treatment and doping of the InGaN/GaN multiple quantum well (MQW) structures and microscopy characterization extended with stress strain state analysis images combined with conventional optical characterization methods. Taiwan group supplied the other two groups by high-quality samples of InGaN/GaN MQWs with various well widths and various In content used as device prototypes.

Latvian group concentrated on photoluminescence excitation spectroscopy, and characterization of charge carrier capture by thermoactivated recombination kinetics in InGaN/GaN heterostructures produced in Taiwan. *Ab initio* calculations of charged point defects in GaN were fulfilled.

Lithuanian group applied a variety of optical characterization methods for the samples produced in Taiwan. The main attention was paid to carrier/exciton localization problem, which was addressed by Monte Carlo simulations of temperature dependencies of luminescence spectral features together with the analysis photoreflectivity spectra and results on site-selective luminescence spectroscopy. Carrier dynamics at high-intensity photoexcitation was studied in order to optimize efficiency of stimulated emission under experimental conditions that are typical for semiconductor laser operation regime.

1.5 Publications

[1] Shih-Wei Feng, En-Chiang Lin, Tsung-Yi Tang, Yung-Chen Cheng, Hsiang-Chen Wang, C. C. Yang, Kung-Jen Ma, Cheng-Hsing Shen, L. C. Chen, K. H. Kim, J. Y. Lin and H. X. Jiang, "Thermal Annealing Effects of an InGaN Film with an Avearge Indium Mole Fraction of 0.31," Applied Physics Letters, Vol. 83, No. 19, pp. 3906–3908, 2003.

[2] Yung-Chen Cheng, Shih-Wei Feng, En-Chiang Lin, C. C. Yang, Cheng-Hua Tseng, Chen Hsu and Kung-Jeng Ma, "Quantum Dot Formation in InGaN/GaN Quantum Well Structures with Silicon Doping and Its Implication in the Mechanisms of Radiative Efficiency Improvement," Physica Status Solidi C, Vol. 0, No. 4, pp. 1093–1096, 2003.

[3] Shih-Wei Feng, Yung-Chen Cheng, En-Chiang Lin, Hsiang-Chen Wang, C. C. Yang, Kung-Jen Ma, Ching-Hsing Shen, L. C. Chen, K. H. Kim, J. Y. Lin, and H. X. Jiang, "Thermal Annealing Effects on the Optical Properties of High-indium InGaN Epi-layers," Physica Status Solidi C, Vol. 0, pp. 26540–2657, 2003.

[4] S. Juršėnas, S. Miasojedovas, G. Kurilčik, A. Žukauskas, Shih-Wei Feng, Yung-Chen Cheng, C. C. Yang, Cheng-Ta Kuo, and Jian-Shihn Tsang, "Quantum-well Thickness Dependence of Stimulated Emission in InGaN/GaN Structures", Physica Status Solidi C Vol. 0, No. 7, pp. 2610–2613, 2003.

[5] Yung-Chen Cheng, En-Chiang Lin, Shih-Wei Feng, Hsiang-Chen Wang, C. C. Yang, Kung-Jen Ma, Chang-Chi Pan, and Jen-Inn Chyi, "Characteristics of Amplified Spontaneous Emission of High Indium Content InGaN/GaN Quantum Wells with Various Silicon Doping Conditions", Physica Status Solidi C, Vol. 0, pp. 2670-2673, 2003.

[6] Yung-Chen Cheng, S. Juršėnas, Shih-Wei Feng, and C.C. Yang, Cheng-Ta Kuo and Jian-Shihn Tsang, "Impact of Post-Growth Thermal Annealing on Emission of InGaN/GaN Multiple Quantum Wells", Phys. Stat. Sol. A, Vol. 201, pp. 221–224 (2004).

[7] Yung-Chen Cheng, En-Chiang Lin, Cheng-Ming Wu, C. C. Yang, Jer-Ren Yang, Andreas Rosenauer, Kung-Jen Ma, Shih-Chen Shi, L. C. Chen, Chang-Chi Pan and Jen-Inn Chyi, "Nanostructures and Carrier Localization Behaviors of Green-luminescence InGaN/GaN Quantum-well Structures of Various Silicon-doping Conditions," (2004) accepted for publication in Applied Physics Letters.

[8] Shih-Wei Feng, Tsung-Yi Tang, Yen-Cheng Lu, Shi-Jiun Liu, En-Chaing Lin, C. C. Yang, Kung-Jen Ma, Ching-Hsing Shen, L. C. Chen, J. Y. Lin and H. X. Jiang, "Cluster Size and Composition Variations in an InGaN Thin Film of Yellow Emission upon Thermal Annealing," (2004) accepted for publication in J. Applied Physics.

[9] K. Kazlauskas, G. Tamulaitis, P. Pobedinskas, A. Zukauskas, Shih-Wei Feng, Yung-Chen Cheng, C. C. Yang, Cheng-Ta Kuo and Jian-Shihn Tsang, "Photoluminescence Linewidth Analysis in InGaN Multiple Quantum Wells Using Monte Carlo Simulation of Exciton Hopping," submitted to Applied Physics Letters

[10] Yung-Chen Cheng, Shih-Wei Feng, C.C. Yang, Cheng-Ta Kuo, Jian-Shihn Tsang, S. Juršėnas, S. Miasojedovas, and A. Žukauskas, "Optical Properties of As-Grown and

Annealed InGaN/GaN Multiple Quantum Wells of Various Well Width," submitted to Semiconductors Science&Technology.

[11] Yung-Chen Cheng, Shih-Wei Feng, C.C. Yang, Cheng-Ta Kuo, Jian-Shihn Tsang, S. Juršėnas, S. Miasojedovas, and A. Žukauskas "Stimulated Emission in InGaN/GaN Multiple Quantum wells With Different Indium Content," submitted to Acta Physica Polonica A.

[12] Yung-Chen Cheng, Cheng-Ming Wu, Meng-Kuo Chen, C. C. Yang, Zhe-Chuan Feng, Gang Alan Li, Jer-Ren Yang, Andreas Rosenauer, and Kung-Jen Ma, "Improvements of InGaN/GaN Quantum Well Interfaces and Radiative Efficiency with InN Interfacial Layers," under revision for publication in Applied Physics Letters.

[13] Hsiang-Chen Wang, Shih-Jiun Lin, Yung-Chen Cheng, C. C. Yang, and Kung-Jen Ma, "Carrier Relaxation in InGaN/GaN Quantum Wells with nm-Scale Cluster Structures", under revision for publication in Applied Physics Letters.

Conference presentations

[14] S. Juršėnas, G. Kurilčik, S. Miasojedovas, and A.Žukauskas, Shih-Wei Feng, Yung-Chen Cheng**,** C. C. Yang, Cheng-Ta Kuo, and Jian-Shihn Tsang, "Stimulated emission in InGaN/GaN structures with different quantum well width", E-MRS Fall meeting (Warsaw, Poland, September 15–19, 2003), p.40.

[15] S. Juršėnas, Yung-Chen Cheng, Shih-Wei Feng, and C.C. Yang, Cheng-Ta Kuo and Jian-Shihn Tsang, "Impact of post-growth thermal annealing on emission of InGaN/GaN multiple quantum wells", E-MRS Fall meeting (Warsaw, Poland, September 15–19, 2003), p.35-36.

[16] S. Juršėnas, G. Kurilčik, S. Miasojedovas, and A.Žukauskas, Shih-Wei Feng, Yung-Chen Cheng**,** C. C. Yang, Cheng-Ta Kuo, and Jian-Shihn Tsang, "Luminescence Spectroscopy of InGaN/GaN Multiple Quantum Wells under High Excitation" 35th Lithuanian National Conference on Physics (Vilnius, Lithuania, June 12–14, 2003), p. 19.

[17] Yung-Chen Cheng, En-Chiang Lin, Shih-Wei Feng, Hsiang-Chen Wang, and C. C. Yang, Kung-Jen Ma, Shih-Chen Shi and L. C. Chen, Chang-Chi Pan and Jen-Inn Chyi, "Effects of Thermal Annealing on InGaN/GaN Quantum Well Structures with Silicon Doping," The Fifth Pacific Rim Conference on Lasers and Electro-Optics CLEO/PR (Taipei, Taiwan, December 15–19, 2003).

[18] Hsiang-Chen Wang, Cheng-Yeh Tsai, Yung-Chen Cheng, En-Chiang Lin, Shih-Wei Feng, C. C. Yang, Kung-Jen Ma, Cheng-Ta Kuo and Jian-Shihn Tsang, "Femtosecond Pump-Prpbe Studies on Carrier Dynamics in InGaN/GaN Quantum Wells with Indium Aggregated Quantum Dot Structures," The Fifth Pacific Rim Conference on Lasers and Electro-Optics CLEO/PR (Taipei, Taiwan, December 15–19, 2003).

[19] Tsung-Yi Tang, Chih-Chung Teng, Shih-Chun Lin, En-Chiang Lin, Meng-Ku Chen, Cheng-Ming Wu, Jiun-Yang Chen, Yung-Chen Cheng, Shih-Wei Feng, C. C. Yang, Kung-Jen Ma, Cheng-Ta Kuo and Jian-Shihn Tsang, "Dependences of Optical and Material Properties on Nominal Indium Content and Well Width IN InGaN/GaN Quantum Well Structures," The Fifth

Pacific Rim Conference on Lasers and Electro-Optics CLEO/PR (Taipei, Taiwan, December 15-19, 2003).

[20] Shih-Wei Feng, En-Chiang Lin, Yung-Chen Cheng, Hsiang-Chen Wang, C. C. Yang, Kung-Jen Ma, Cheng-Hsing Shen, L. C. Chen, K. H. Kim, J. Y. Lin and H. X. Jiang, "Quantum Dot Structures and Optical Properties of a High-Indium InGaN Film," The Fifth Pacific Rim Conference on Lasers and Electro-Optics CLEO/PR (Taipei, Taiwan, December 15–19, 2003).

[21] Shih-Wei Feng, En-Chiang Lin, Tsung-Yi Tang, Yung-Chen Cheng, Hsiang-Chen Wang, C. C. Yang, Kung-Jen Ma, Ching-Hsing Shen, L. C. Chen, K. H. Kim, J. Y. Lin and H. X. Jiang, "Optical and Nano-Structures of InGaN Films with Average Indium Contents Higher Than 30 %," Materials Research Society's 2003 Fall Meeting (Boston, USA, December 1–5, 2003).

[22] Yung-Chen Cheng, En-Chiang Lin, Hsiang-Chen Wang, C. C. Yang, Kung-Jen Ma, Chang-Chi Pan and Jen-Inn Chyi, "Gain Characteristics of InGaN/GaN Quantum Well Structures with Various Silicon Doping Conditions," Materials Research Society's 2003 Fall Meeting (Boston, USA, December 1–5, 2003).

[23] Hsiang-Chen Wang, Cheng-Yeh Tsai, Yung-Chen Cheng, En-Chiang Lin, C. C. Yang, Kung-Jen Ma, Cheng-Ta Kuo and Jian-Shihn Tsang, "Study on Ultra-fast Carrier Dynamics in InGaN/GaN Quantum Wells with Indium Aggregated Quantum Dot Structures," Materials Research Society's 2003 Fall Meeting (Boston, USA, December 1–5, 2003).

[24] M. Springis, P.Kulis, I.Tale, "Thermoactivation and Spectroscopy of Charge Localization States in a InGaN/GaN Quantum Well," NATO Advanced Research Workshop (Vilnius, Lithuania, June 17–21, 2003), p.22.

[25] Yung-Chen Cheng, Horng-Shyang Chen, C. C. Yang, Z. C. Feng, and Gang Alan Li, "Effects of interface thin layers in InGaN/GaN quantum well structures," The Fifth International Symposium on Blue Laser and Light Emitting Diodes ISBLLED-2004, (Gyeongju, Korea, March 15–19, 2004).

[26] Yung-Chen Cheng, En-Chiang Lin, C. C. Yang, Jer-Ren Yang, Andreas Rosenauer, Kung-Jen Ma, Chang-Chi Pan, and Jen-Inn Chyi, "Mechanisms of emission enhancement with silicon doping in InGaN/GaN quantum wells," The Fifth International Symposium on Blue Laser and Light Emitting Diodes ISBLLED-2004 (Gyeongju, Korea, March 15–19, 2004).

[27] Yung-Chen Cheng, En-Chiang Lin, C. C. Yang, Jer-Ren Yang, Andreas Rosenauer, Kung-Jen Ma, Shih-Chen Shi, and L. C. Chen, "Quantum Dot Structures in Silicon-doped InGaN/GaN Quantum Wells," 2004 Nano Materials for Defense Applications Symposium & US/Taiwan Workshop (Maui, Hawaii, US, February 19–26, 2004).

[28] Shih-Wei Feng, C. C. Yang, Kung-Jen Ma, Ching-Hsing Shen, L. C. Chen, K. H. Kim, J. Y. Lin, and H. X. Jiang, "InGaN Quantum Dot Structures and Their Optical Properties in InGaN Thin Films," Photonics West (San Jose, USA, January 2004).

[29] Yung-Chen Cheng, En-Chiang Lin, Meng-Kuo Chen, Cheng-Ming Wu, C. C. Yang, and Kung-Jen Ma, "Optimum design of silicon doping for emission enhancement of InGaN/GaN quantum well light-emitting devices," Conference on Lasers and Electro-Optics (San Franscisco, May, 2004).

[30] Yung-Chen Cheng, En-Chiang Lin, Meng-Kuo Chen, Cheng-Ming Wu, C. C. Yang, and Kung-Jen Ma, "Optimum design of silicon doping for emission enhancement of InGaN/GaN quantum well light-emitting devices," Conference on Lasers and Electro-Optics (San Franscisco, May, 2004).

[31] I.Tale, M. Piesins and C.C.Yang. Thermoactivation spectroscopy of charge localization states in InGaN/GaN Quantum Well. International Workshop on Nitride Semiconductors (Pittsburgh, PA, USA, July 19–23, 2004).

[32] Guļāns, R. A. Evarestov, I. Tāle, C.C Yang. "LCAO calculation of defects in GaN," International Workshop on Nitride Semiconductors (Pittsburgh, PA, USA, July 19–23, 2004).

[33] A.Sharakovsky, I.Tale, M.Springis, S.Jursenas, C.C.Yang, "Spectroscopy of Charge Localization States in InGaN/GaN Multiquantum Wells,"ICDIM 2004 (Riga, Latvia, July, 2004).

[34] Guļāns, R. A. Evarestov, I. Tāle, C.C. Yang. Ab initio calculations of charged point defects in GaN. Abstracts of ICDIM 2004 (Riga, Latvia, July, 2004).

[35] A. Zukauskas, K. Kazlauskas, G. Tamulaitis, J. Mickevičius, S. Jursėnas, G. Kurilcik, S. Miasojedovas, M. Springis, I. Tale, Yung-Chen Cheng, Hsiang-Cheng Wang, Chi-Feng Huang, and C. C. Yang, "Carrier Localization Effect in Polarized InGaN/GaN Multiple Quantum Wells"**,** International Workshop on Nitride Semiconductors (Pittsburgh, PA, USA, July 19–23, 2004).

[36] Hsiang-Chen Wang, Shih-Chun Lin, Yen-Chen Lu, Yung-Chen Cheng, C. C. Yang, and Kung-Jen Ma, "Ultrafast Carrier Relaxation in InGaN/GaN Quantum Wells with nm-scale Cluster Structure," International Workshop on Nitride Semiconductors (Pittsburgh, PA, USA, July 19–23, 2004).

[37] Yung-Chen Cheng, Meng-Kuo Chen, Cheng-Ming Wu, C. C. Yang, Jer-Ren Yang, Andreas Rosenauer, Kung-Jen Ma, Shih-Chen Shi, L. C. Chen, Chang-Chi Pan and Jen-Inn Chyi, "Differences in Nanostructure and Carrier Localization Behavior of InGaN/GaN Quantum-well Structures with Different Silicon-doping Conditions," . International Workshop on Nitride Semiconductors (Pittsburgh, PA, USA, July 19–23, 2004).

[38] Yung-Chen Cheng, Cheng-Ming Wu, C. C. Yang, Zhe-Chuan Feng, Gang Alan Li, Andreas Rosenauer, and Kung-Jen Ma, "Improvements of InGaN/GaN Quantum Well Quality and Radiative Efficiency with InN Interfacial Layers," . International Workshop on Nitride Semiconductors (Pittsburgh, PA, USA, July 19–23, 2004).

[39] K. Kazlauskas, G. Tamulaitis, P. Pobedinskas, A. Zukauskas, Chi-Feng Huang, Yung-Chen Cheng, Hsiang-Chen Huang, and C. C. Yang, "Photoluminescence temperature behavior and Monte Carlo simulation of exciton hopping in InGaN multiple quantum wells," . International Workshop on Nitride Semiconductors (Pittsburgh, PA, USA, July 19–23, 2004).

[40] Yung-Chen Cheng, Shih-Wei Feng, C.C. Yang, Cheng-Ta Kuo, Jian-Shihn Tsang, S. Juršėnas, S. Miasojedovas, and A. Žukauskas "Stimulated emission in InGaN/GaN multiple quantum wells with different indium content", Int. Symph. Ultrafast phenomena in semiconductors, UFPS-12 (Vilnius, Lithuania, August, 22–25, 2004).

1.6 Research plan for year 2004-2005

Recognition and quantitative theoretical description of localized exciton and defect states in InGaN/GaN device quality structures

Taiwan group

Materials characterization of InGaN/GaN quantum dots;

- Stimulated emission measurements for optical gain spectrum and optical gain coefficient calibrations in various In-content and various Si-doping InGaN/GaN multiple quantum well and quantum dot structures;
- Study of optical gain coefficient dependence on indium-aggregated cluster density, cluster size and threading dislocation density;
- Waveguide implementations.

Latvian group

- Site selective and photoluminescecnce excitation spectroscopy of InGaN/GaN heterostructures
- Electron paramagnetic resonance studies of films in equilibrium and radiation excited states;
- Study of the thermostimulated luminescence and thermostimulated depolarization currents versus temperature in III-N samples of different structural quality and composition;
- *Ab –initio* calculations of the electron structure of In quantum dots – like structures in GaN.

Lithuanian group:

- Monte Carlo simulation of luminecence transients due to exciton hopping in partially disordered nitride alloys;
- Modeling of the impact of Si doping on of exciton hopping In disordered InGaN/GaN heterostructures;
- Investigation of the impact of band potential fluctuations on stimulated emission of highly excited in InGaN/GaN MQWs (including Si doped structures) by picosecond time-reslved photoluminescence measurements;

II. Detailed description of the results

2.1 OPTICAL PROPERTIES OF AS-GROWN AND ANNEALED InGaN/GaN MULTIPLE QUANTUM WELLS OF VARIOUS WELL WIDTH

by

Yung-Chen Cheng, Shih-Wei Feng, C.C. Yang,
Graduate Institute of Electro-Optical Engineering and Department of Electrical Engineering, National Taiwan University 1, Roosevelt Road, Sec. 4, Taipei, Taiwan, R.O.C
Cheng-Ta Kuo, Jian-Shihn Tsang,
Advanced Epitaxy Technology Inc., Hsinchu Industrial Park, Hsinchu, Taiwan, R.O.C
S. Juršėnas, S. Miasojedovas, and A.Žukauskas
Institute of Materials Science and Applied Research, Vilnius University, Saulėtekio al. 9, Building III, LT-10222 Vilnius, Lithuania

Abstract
Site-selective photoluminescence, photoluminescence excitation and time-resolved luminescence in as-grown and thermally treated $In_{0.15}Ga_{0.85}N$/GaN multiple quantum wells (MQWs) was investigated as a function of well width in the temperature range of 10–300 K. Thermal annealing at 800 ºC for 30 min monitored by microstructure imaging was shown to result in an alteration of MQWs optical properties intricately depending on the well thickness. The observed blue shift of the luminescence band and pronounced changes in the absorbance indicate on remarkable interdiffusion of indium at the quantum well–barrier interface for MQWs with thin (2 nm) wells. Meanwhile for thicker (3 nm) wells, a pronounced red shift of the luminescence band and an increase in the luminescence decay time was observed and attributed to electron–hole wavefunction separation facilitated by the smoothened band potential profile. In the thickest wells (4 nm), annealing resulted in even more pronounced improvement of microstructure, which led to a noticeable reduction of the localization energy of the electronic excitations (an annealing-invoked luminescence peak blue shift that overweighs the red one caused by built-in field) and to suppression of nonradiative recombination (an increase in luminescence efficiency). The results are accounted for in terms of annealing-invoked In–Ga interdiffusion, which behaves as either diffusion of indium to barriers or "up-hill" diffusion within the wells depending on the well width.

2.1.1. Introduction

InGaN-based multiple quantum wells (MQWs) are the key structures for manufacturing of violet, blue, and green light emitting diodes and laser diodes [1,2]. Fabrication of the light-emitting devices requires further optimization of the structures for increased efficiency and lifetime. Thermal treatment is one of the technological factors that may facilitate optimization of active, barrier, and contact layers. Typically during the epitaxial growth of InGaN/GaN structures and during the fabrication of devices, the structures undergo several high-temperature impacts [1]. However, thermal treatment introduced for a particular layer might have an unexpected impact on the other layers. In particular, thermal treatment can change the distribution of the indium composition and influence strain in the quantum wells through ordinary diffusion [3–5] and "up-hill" strain-induced diffusion [6–9].

Usually thermal annealing is related to indium and gallium interdiffusion across the interface of quantum-well and barrier layers [3–5]. This results in a blue shift of the photoluminescence (PL) and absorbance spectra [5]. A complete merging of the barrier and well layers has been observed in an InGaN/GaN structure after annealing at high temperature [4]. On the other hand, In–Ga interdiffusion in InGaN alloys is rather intricate because of immiscibility of InN and GaN materials what can result in phase separation in InGaN layers [6,7]. Since InGaN alloys usually are grown at temperatures below 1473 K, the critical temperature above which the InN–GaN system is completely miscible [10,11], in all InGaN alloys phase separation is expected based on thermodynamics considerations. The phenomenon of InGaN phase separation [6–14] is of considerable interest, since InN-rich regions were reported to play a crucial role in light generation in nitride-based light emitting structures [15–19]. Phase separation has been observed using several growth techniques, preferably in thick films [6–9,12]. The observed phase separation is evidently driven by strain due to the mixing of the two lattice mismatched components of the InGaN alloy system. Indium atoms are expelled from the InGaN lattice what results in an occurrence of an alloy of different composition and in reduced strain energy of the system. It has been predicted that for a standard growth temperature, spinodal decomposition occurs for indium concentration above 20% [10,11]. Post-growth thermal annealing was reported to facilitate formation of indium-rich regions in InGaN quantum wells [6–9,13]. On the other hand, thermal annealing can lead to redistribution of strain energy and reduced phase separation, which is sensitive to strain effects. Both phase separation and strain effects are expected to enhance with increasing the InGaN well width. Therefore, the annealing-induced In diffusion mechanism can be well-width dependent.

In the present work, the impact of post growth thermal treatment on optical properties of InGaN/GaN MQWs with various well layer thicknesses was investigated. As grown and annealed samples, which display different images of high-resolution transmittance electron microscopy (HRTEM), were investigated by site-selective PL, observation-energy-selective photoluminescence excitation (PLE), temperature dependent PL, and time-resolved photoluminescence (TRPL). Distinct changes of the MQWs optical properties for the samples of different well layer thickness were linked with the microstructure changes invoked by thermal treatment.

2.1.2. Experimental

The samples were grown on *c*-plane sapphire by metalorganic chemical vapour deposition. Following the deposition of 30-nm GaN buffer layer and a 2.3-μm GaN layer, MQW structures consisting of five pairs of $In_{0.15}Ga_{0.85}N$ well and 10 nm-thick GaN barrier were grown. Three samples with different well widths of 2, 3, and 4 nm were prepared and referred to as samples w20, w30 and w40, respectively. The growth temperatures were 1010 and 720 ^{0}C for GaN and InGaN, respectively. A set of three as-grown samples and three counterpart ones thermally annealed in a quartz tube furnace at 800 $^\circ$C in nitrogen ambient for 30 min was investigated.

A cw He–Cd laser (photon energy $h\nu = 3.812$ eV) was used for PL excitation. The samples were placed in a cryostat for temperature-dependent measurements. For TRPL measurements, a Verdi^{TM}-laser pumped mode-locked Ti:sapphire laser with 100 fs pulse width and 76 MHz pulse repetition rate with frequency doubling by a BBO crystal was used ($h\nu = 3.177$ eV). Luminescence from the sample was collected and focused into a spectrometer prior to imaging in a Hamamatsu streak camera. The temporal resolution of the operation mode was 4.7 ps. PLE experiments were conducted using quasi-monochromatic excitation light source from a xenon lamp dispersed by a 0.15-m monochromator. The bandwidth of the excitation light from the xenon lamp was set at less than 3 nm.

HRTEM investigations were carried out by a 200KeV Philips CM 200 and a 300KeV JEM 3010 microscopes. All the high-resolution micrographs were taken at Scherzer defocus and the sample was viewed along a [11-20] zone axis. The 300keV JEM 3010 microscope was equipped with a 2k×2k slow-scan CCD camera and Gatan Imaging Filter.

2.1.3. Results

A High-Resolution Transmission Electron Microscopy of InGaN/GaN MQWs

According to microstructure analysis performed in the first year study (see Report 2002-2003, Chapter 2.1), HRTM analysis of MQWs was performed for as-grown and annealed samples of various well thicknesses.

The periodic structure of MQWs can be clearly resolved in all images. Typically for ternary InGaN system, the In concentration and strain are rather randomly distributed along MQW layers. Although all our as-grown samples nominally contain the same molar fraction of indium, actual phase separation pattern in the layers of various thickness might be different. Growth of MQWs of a lager thickness requires longer time, thus the quantum well layers have more time for strain relaxation and phase separation. Eventually, more pronounced fluctuations of indium content are expected. This can result in different impact of thermal annealing. The w20 as-grown sample exhibits rather diffusive distribution of strain and indium content, although distinct positions of QWs can be identified. After thermal annealing, the dark areas in the images related to the QWs enhance and occupy a remarkable part of the barrier region. This allows us to make a suggestion about indium interdiffusion in to the barriers and/or enhancement of strained interface regions due to thermal annealing in thin w20 layers.

Thicker MQWs w30 show opposite structural changes under thermal treatment. After thermal treatment, initially large and randomly distributed around QWs dark regions become thinner. This suggests “up-hill” diffusion of indium and/or reduction of strain in the interface regions of thick InGaN/GaN MQWs.

To verify the suggestions that follow from the analysis of microstructure revealed by HRTEM images, below an impact of thermal treatment on optical properties of the MQWs is considered in detail.

B Low temperature site-selective PL and PLE spectroscopy

Solid lines on the left-hand side of Fig. 1 show normalized PL spectra of as-grown InGaN/GaN MQW samples obtained at 10 K. The main luminescence spectral properties are typical of low-temperature emission in InGaN/GaN MQWs [16,18,20]. The luminescence spectrum of the w20 sample (Fig. 1(a)) consists of a main band at 2.958 eV, which can be attributed to localized exciton states, and its phonon replica located on the low-energy wing at about 2.865 eV. The band at the high-energy wing of the main luminescence band might be related to shallow impurity related centres [20]. The shape of the spectrum weakly depends on the excitation photon energy (not shown). Meanwhile, the luminescence intensity rapidly decreases with tuning of the excitation photon energy below 3.1 eV as it is seen in the PLE spectra. With increasing the well width of the as-grown samples, the luminescence spectra steadily redshifts with the main peak positioned at 2.767 eV and 2.589 eV for samples w30 (Fig. 1(b)) and w40 (Fig. 1(c)), respectively. The red shift is contributed by several impacts: i) a decrease in quantum confinement energy, ii) the quantum confined Stark effect (QCSE) due to an increase in electron-hole wave function separation caused by built-in field, and iii) deeper localization of the electronic excitations due to an enhancement of disorder-related fluctuations of the band potential profile. At the same time, the bandwidth is seen to decrease with the well width: the estimated full with at half magnitude (FWHM) is 128 meV, 108 meV, and 89 meV for the samples w20, w30, and w40, respectively. The shape of the luminescence

band becomes more sensitive to the excitation photon energy with increasing the well width (not shown): the band broadens and blueshifts with an increase of the excitation photon energy. This can be attributed to an enhancement of band potential fluctuations related to growth-time dependent phase separation on the growth surface [8,9].

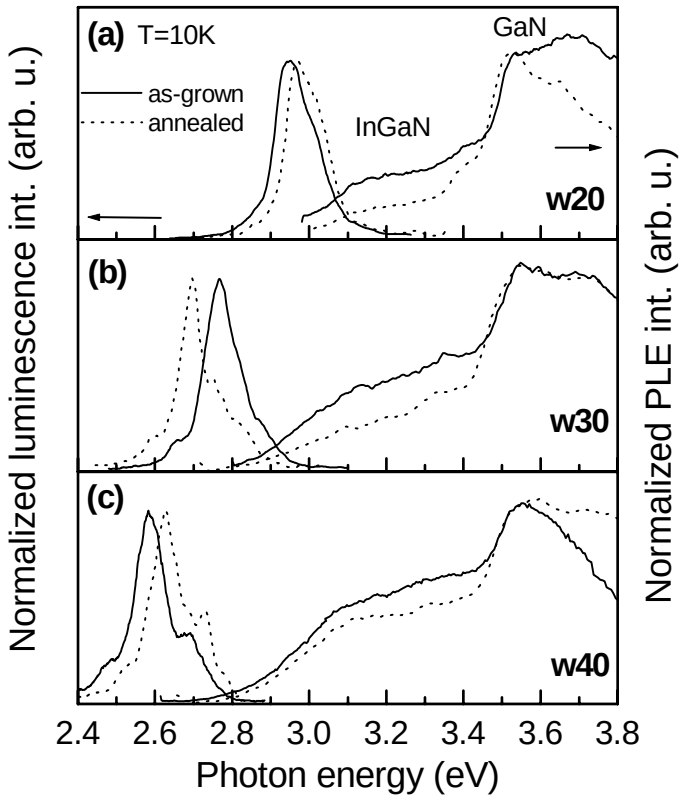

Figure 1. Normalized photoluminescence spectra and photoluminescence excitation spectra of as-grown (solid line) and annealed (dotted line) InGaN/GaN MQWs: w20 (a), w30 (b) and w40 (c), measured at 10 K.

Solid lines on the right-hand side of Fig. 1 show PLE spectra of the w20, w30, and w40 as-grown samples. The PLE spectra exhibit typical dependences of MQW structures with spectral variation in optical density of the QW (InGaN) and barrier (GaN) materials reflected. The PLE signal is much stronger for the excitation photon energy above 3.5 eV due to the larger thickness of the barrier layer (10 nm). The boundary between the PLE features of InGaN and GaN layers is sharp due to the edge of excitonic absorbance in GaN. The absorbance edge of InGaN material below 3.1 eV is less steep indicating on the presence of compositional fluctuations, which were seen in the HRTEM images.

With an increase in well width from 2 nm to 4 nm, pronounced changes can be revealed in the well absorbance region: i) an increase in PLE signal due to increased optical density of the InGaN layer; ii) a redshift of about 66 meV that is in line with the quantum confinement effect (note, that built-in electric field can also affect excitonic absorbance spectrum); iii) a pronounced sensitivity of the PLE signal intensity to the observation photon energy (not shown). The latter effect is due to aforementioned sensitivity of the shape of the luminescence band to the excitation photon energy in thicker wells, what is an indication of increased disorder.

In addition, a pronounced difference in the PLE signal caused by absorbance in the GaN barrier layers ($h\nu > 3.50$ eV) is peculiar for different well widths. Instead of a rising dependence, which is predictable for a MQW structure of good quality, a significant decline of the PLE signal for the excitation photon energy above 3.50 eV is observed in the as-grown structures with increased well width. This can be attributed to an enhancement of nonradiative capture of just photogenerated excitons (electrons and holes) with a higher initial excess

energy. To produce luminescence from the QW states, the excitons (carriers) excited in the barrier layer are to be captured in the well. However, excitations with a larger excess energy have a smaller well-capture probability and, consequently, a higher overall probability of trapping to nonradiative centres. Thus, the decline in the PLE spectra for $h\nu > 3.50$ eV can be explained under assumption that increased well width results not only in reduced quality of the well material but of the barrier and/or interface also. This is in line with the HRTEM images (Fig. 2(a)–(c)) where an increased patterning of the barrier layers in the as-grown samples with increased well width can be distinguished.

Dotted lines in Fig. 1 show normalized PL and PLE spectra of annealed InGaN/GaN MQWs measured at 10 K. The PL spectrum of the annealed w20 sample blueshifts by about 20 meV in comparison with the as-grown one (Fig. 1(a)). The PL spectrum of the annealed w30 sample redshifts by about 71 meV, while that of the w40 sample blueshifts by about 45 meV. This indicates on an intricate impact of thermal treatment on the luminescence properties of MQWs of various well widths.

The PLE spectra (dotted lines on the right-hand side of Fig. 1) show significant spectral changes as well. (The spectra are normalized at 3.50 eV to reveal spectral changes occurring upon annealing.) The most pronounced impact of thermal treatment appears for the thin-well sample w20 (Fig. 1(a)). A decline of the spectral dependence of the PLE signal in the barrier spectral region at $h\nu > 3.50$ eV evidences on a remarkable increase in nonradiative trap density. This is in line with significant reduction of the luminescence efficiency (see below). Additionally by detailed comparison of the spectra, a blue shift of the PLE feature due to wells at the absorbance edge can be distinguished concurrently with the blue shift of the PL line. These observations support a suggestion drown from the microstructure analysis that thermal treatment results in In interdiffusion from the well layers to the barriers [3–5].

The impact of thermal treatment on the PLE spectra of the thicker QW layers is of opposite character (Fig. 1(b), (c)). The sample w30 shows little changes in the PLE spectrum in the barrier spectral region $h\nu > 3.50$ eV, while the even thicker w40 sample shows an opposite trend: thermal treatment results in a flatter spectral dependence indicating on reduction of the nonradiative traps. Again, this is in line with the narrowing of the dark regions in the HRTM images (Fig 1(c), (f)). The QW absorbance edge becomes flatter for the w30 sample and steeper for the w40 sample. As discussed below, such a behaviour might be due to several impacts such as, indium diffusion, increase in disorder due to composition fluctuations, and electron–hole wavefunction separation due to built-in field.

C Temperature dependent PL and TRPL

The temperature variations of the PL peak position in the three pairs of the as-grown and annealed samples are shown in Fig. 2. Both before and after thermal annealing, the characteristic “S-shape” variation of the PL peak can be distinguished in each case indicating on migration of excitations within spectrally and spatially disordered system [21,22]. In both the as-grown and annealed samples, the amplitude of the initial decrease in peak energy diminishes with the well thickness. As revealed by Monte Carlo simulation of exciton hopping [21,22], this can be attributed to an increase in spatial separation between the localized states in thicker wells what is in line with enhanced In segregation seen in HRTEM images. Similar behaviour might be caused by reduced lifetime of the excitons or carriers; however, our TRPL results indicate that lifetime increases with the well width. The “S-shape” becomes more pronounced in the annealed samples. Again, this can be attributed to a decreased spatial separation between the localized states and/or increased lifetime. To our opinion in the thin wells (w20), the major effect is due to increased lifetime (see Fig.4(a)), whereas in the thicker wells (w30 and w40) both effects might be important.

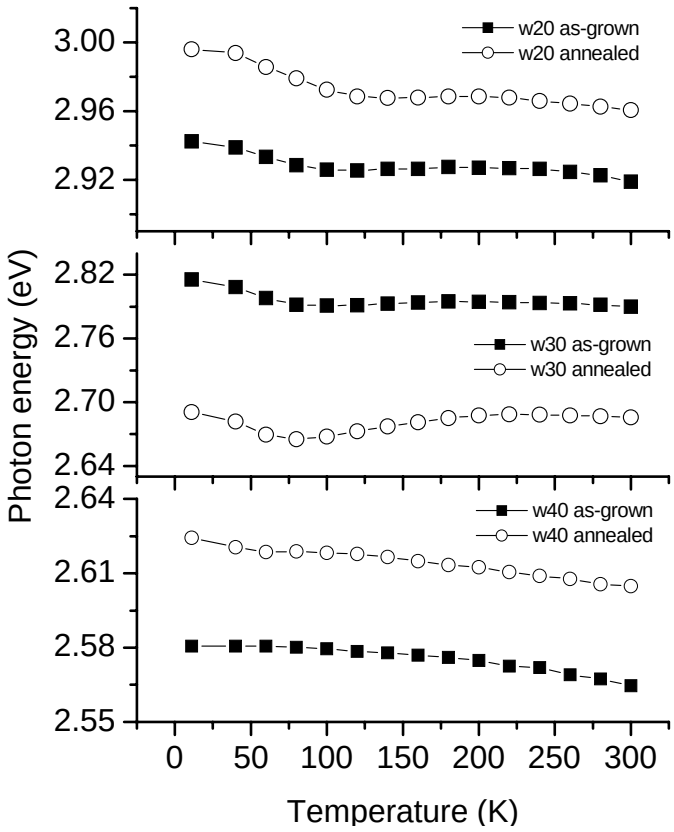

Figure 2. Variations of PL peak positions versus temperature of as-grown and annealed samples: w20 (a), w30 (b) and w40 (c).

Figure 3 shows temperature-dependent variations of the integrated PL intensity in the as-grown and annealed samples. Thermal treatment is seen to cause a significant reduction in PL intensity in the w20 sample (Fig. 3(a)), in agreement with the suggestion on In interdiffusion and consequent degradation of the barriers and interfaces. Correspondingly, the flatter temperature dependence in the annealed sample is an indication of a larger energy required for delocalization, which facilitates nonradiative recombination [23]. Sample w30 shows similar temperature dynamics (Fig. 3(b)), however without a remarkable change in the activation energy. This can be attributed to an increased role of electron–hole wavefunction separation due to built-in field in thicker wells what agrees with the observed red shift of the PL peak position (Fig. 1(b)). We suggest that such a separation is facilitated by a smoother potential profile in the annealed wells as evidenced by the HRTEM images and temperature dependence of the PL peak position. With further increase in well thickness (sample w40), the principal impact of annealing is an increase of the PL intensity in the entire range of temperatures. In combination with the blue shift of the PL peak position (Fig. 1(c)), such an increase can be attributed to a significant smoothing of the band potential profile and a subsequent decrease of the localization energy. An additional increase in PL intensity might be caused by a reduced number of nonradiative centres in the barrier layers and interfaces what is in agreement with the HRTEM images and PLE spectra.

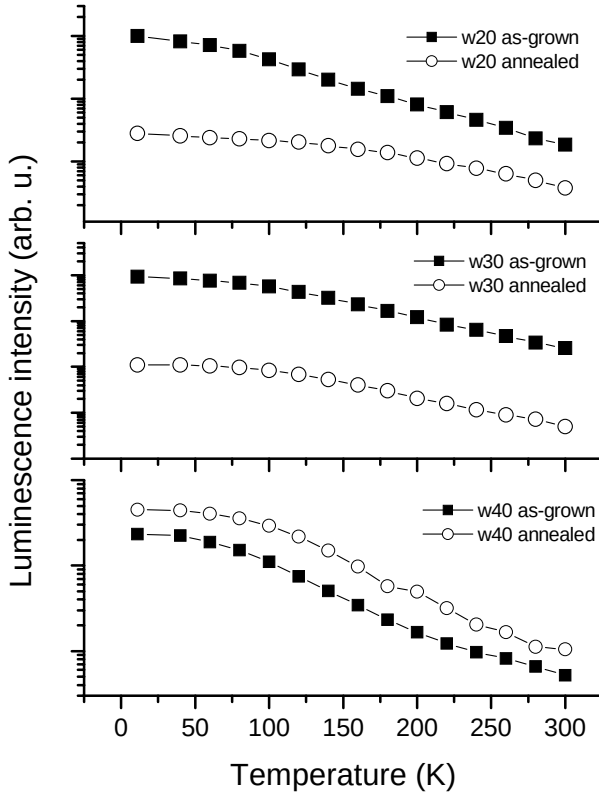

Figure 3. Variations of PL intensities versus temperature of as-grown and annealed samples: w20 (a), w30 (b) and w40 (c).

Figure 4 shows PL decay time at the PL spectral peaks as a function of temperature in the as-grown and annealed samples [14]. (In the annealed w40 sample, the PL decay time becomes too long to be measured by our technique.) The low-temperature lifetime of the as-grown samples rapidly increases with the well width and is equal to 1.8 ns, 9 ns, and 137 ns for w20, w30, and w40 samples, respectively. This increase is obviously due to spatial separation of electron and hole wavefunctions in thicker wells (QCSE) [24,25]. This is in line with the increase in Stokes shift with the well width (Fig. 1). Thermal annealing generally results in an increase of carrier lifetime, however, with the peculiarities dependent on the well width. In the w20 sample, the lifetime alters negligibly at low temperature and exhibits a remarkable increase at elevated temperatures. This effect agrees with the temperature dynamics of the PL intensity in that annealing of a thin well results in an enhancement of potential fluctuations and in a higher energy required for delocalization, which initiates the nonradiative process [23]. Interestingly, despite the unchanged lifetime at low temperature, the annealed sample exhibits a lower PL efficiency (Fig. 3(a)), probably because of reduced rate of carrier capture to the well due to degraded barriers and/or interfaces. Contrarily, the thicker wells (w30) show a remarkable increase in low-temperature lifetime after thermal annealing, the difference between the as-grown and annealed samples disappearing with temperature (Fig. 3(b)). Such behaviour might be accounted for by an increased electron–hole wavefunction separation at low temperatures due to increased carrier/exciton diffusivity in the annealed sample. At elevated temperatures, annealing results in negligible changes of lifetime, since the excitations are delocalised. In the thickest sample (w40), localization energy is higher and annealing facilitates the QCSE in the entire temperature range.

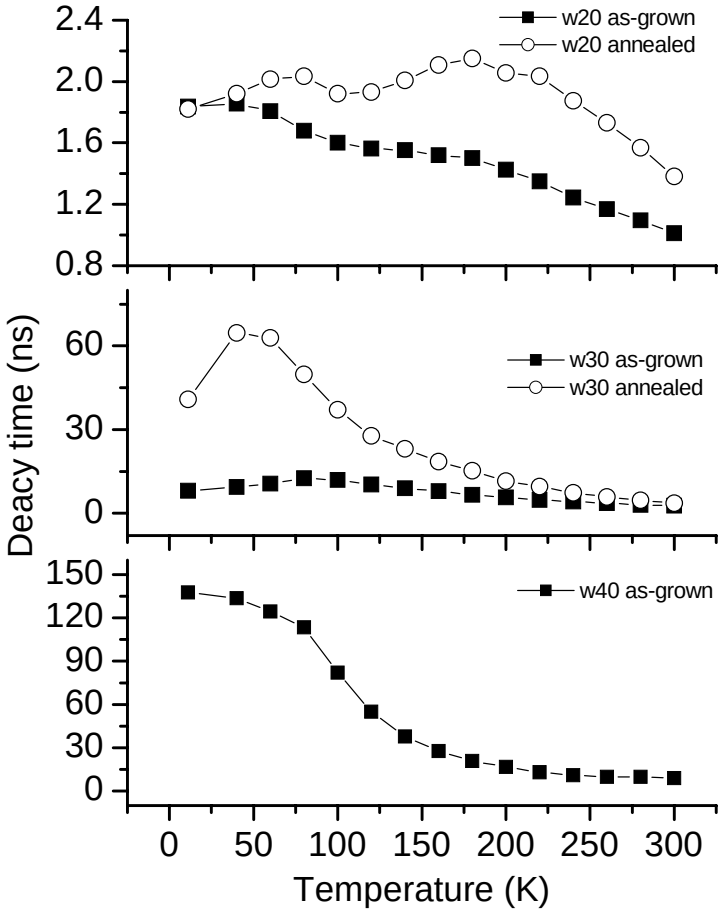

Figure 4. Variations of PL decay times versus temperature of as-grown and annealed samples: w20 (a), w30 (b). That of the as-grown w40 is also shown.

2.1.4. Discussion

Our results on HRTEM, PL, PLE, and TRPL in InGaN/GaN MQWs revealed dynamics of radiative and nonradiative processes with the well thickness and the impact of thermal treatment, which was shown to essentially depend on the quantum well width.

Quantum well width dynamics of recombination processes in InGaN/GaN MQWs is usually explained by the QSCE and inhomogeneous distribution of indium as well as by nonradiative centres due to structural and point defects [15–17, 24–26]. Basically, dynamics of the QSCE with the well width is enough understood for a smooth band potential profile [24,25]. Meanwhile, inhomogeneous distribution of indium, which results in fluctuations of the band potential profile, displays a much more intricate dependence on the well width. There are several studies on accumulation of indium atoms on the growth surface and generation of misfit dislocations with increasing the thickness of the InGaN layer [27,28]. The concurrent plastic relaxation cannot be complete and homogeneous in all regions of the InGaN well, resulting in an inhomogeneous strain distribution within the layer. The inhomogeneous strain distribution could, in turn, enhance the local diffusion of indium atoms and thereby spinodally increases the composition fluctuations. Under favourable conditions, these fluctuations may result in phase separation [8,9]. Phase separation requires long-range diffusion and a correlation should exist between phase separation and the growth time. The larger the layer thickness, the longer growth time is required, thus the quantum well layer has a longer time for strain relaxation and a more pronounced variation in indium content is expected. Our data on optical properties of InGaN/GaN MQWs infer that increasing the well width results in i) increased potential profile fluctuations, which are known to remarkably influence the migration of electronic excitations, ii) a modified nomenclature of nonradiative centres due to

indium decomposition and modification of interfaces, iii) enhanced spatial separation of the electron and hole wavefunctions in the wells.

Increased fluctuations of the band potential profile are evidenced by enhanced patterning of the HRTM images, by sensitivity of the PL spectra to the excitation photon energy, sensitivity of the PLE spectra to the observation photon energy, flattening of the well absorbance edge monitored by PLE, and smoothening of the "S-shape" temperature dependence of PL with the increase in the well thickness. The decrease in carrier capture efficiency to the wells due to nonradiative recombination is clearly monitored by changes in the PLE spectrum in the barrier region. Enhanced spatial separation of the electron and hole wavefunctions is evidenced by a significant increase in carrier/exciton lifetime and by a increase in Stokes shift of PL, with both increases partially attributed to increased potential fluctuations. All these observations clearly indicate on an increase in disorder with an increase of the well width.

Differences in degree of disorder of as-grown samples with various well widths leads to different impact of thermal annealing on luminescence from localized states. Since the average indium concentration in our samples is of 15%, only slightly below the critical value [10,11], one can expect different trends in diffusion related processes (diffusion or spinodal decomposition) invoked by thermal treatment. Our data infers that thermal annealing, which basically results in thermally activated In–Ga interdiffusion including "up-hill" strain-induced diffusion and spinodal decomposition, affects microstructure and strain in the wells, barriers and interfaces. Eventually, thermal annealing modifies i) the efficiency of carrier capture to the wells, ii) electron–hole wavefunction separation within the wells, and iii) nonradiative recombination rate, i.e. the basic processes, which govern the quantum efficiency of light generation in InGaN/GaN MQWs.

After thermal annealing, thinner samples that initially are of the best structural and optical quality are heavily deteriorated. We attribute this effect to indium interdiffusion into the barrier layers, what is monitored by the HRTM images. Annealing leads to changes in indium content as evidenced by the blueshift of the InGaN related emission and absorption bands. Indium interdiffusion also results in formation of a large amount of nonradiative defects both in the well and barrier, what is confirmed by a significant reduction in luminescence efficiency and by modification of the PLE spectra in the barrier region. Meanwhile, no indications of changes in spatial separation of electrons and holes were distinguished, probably because of the well thickness too small for the QSCE to manifest itself.

Thicker as-grown samples are already much more disordered due to indium segregation. This leads to an increase in the number of surface related defects. Increased thickness results in a noticeable enhancement of the QSCE, what is monitored by the increased carrier lifetime, decreased PL efficiency, and red shift of the PL peak. Annealing seems to improve materials quality and to make potential profile smoother. The smoother potential profile facilitates electron–hole spatial separation, which results in the enhanced QSCE (an increase in the carrier/exciton lifetime, a decrease in PL efficiency, and the red shift of the PL band).

For the thickest samples investigated, thermal annealing results in even more significant improvement of microstructure, what is evidenced by the narrowing of well-related dark regions in the HRTM images, as well as by modification of the barrier related PLE spectrum. This implies that indium is preferentially reorganized in the InGaN layers rather than diffused into GaN barriers. Consequent smoothening of the well potential profile leads to an increased electron–hole spatial separation due to built-in field. However the blue shift of the PL peak and an increase in PL efficiency show that annealing invokes a competing impact that outbalances the manifestation of the QCSE. We attribute this impact to improved

microstructure, which results in shallower localization and remedy of nonradiative-recombination centres.

2.1.5. Conclusions

Summarizing, temperature dependent site-selective PL, PLE, and TRPL study of three pairs of as-grown and annealed at 800º C for 30 min $In_{0.15}Ga_{0.85}N$/GaN MQWs with the well widths of 2, 3, and 4 nm were performed. Our results imply a nontrivial dependence of MQWs emission properties on thermal treatment. Differences in degree of disorder in as-grown samples of various well width leads to different impact of thermal annealing on luminescence from localized states. The blue shift of the PL peak and pronounced changes in the absorbance indicate a remarkable interdiffusion of indium at the quantum well barrier interface for thin MQWs. While the pronounced red shift in PL and an increase in the excitation lifetime in thicker MQWs is attributed to manifestation of the QCSE due to built-in field. Also, MWQs of larger thickness were shown to possess larger variations in potential profile and a larger amount of structural defects. *The performed optical and microstructure analysis evidences on an improvement of the MQW structural quality and increased emission efficiency in the thicker structures upon post growth thermal annealing*.

References

[1] Nakamura S and Fasol G 1997 *The Blue Laser Diode: GaN Based Light Emitters and Lasers* (Berlin, Springer).

[2] Žukauskas A, Shur M S, and Gaska R 2002 *Introduction to Solid-State Lighting* (New York, Wiley).

[3] Tsang J-S, Guo J-D, Chan S-H, Feng M-S and Chang C-Y, 1997 *Jpn. J. Appl. Phys*. **36** 1728.

[4] Romano L T, McCluskey M D., Van de Walle C G, Northrup J E, Bour D P, Kneissl M, Suski T and Jun J 1999 *Appl. Phys. Lett.* 75 3950.

[5] Chou C-C, Lee C-M and Chyj J-I 2001 *Appl. Phys. Lett.* **78** 314.

[6] Singh R, Doppalapudi D, Moustakas T D and Romano L T 1997 *Appl. Phys. Lett.* **70**, 1089.

[7] McCluskey M D, Romano L T, Krusor B S, Bour D P, Johnson N M and Brennan S 1998 *Appl. Phys. Lett.* **72**, 1730.

[8] Doppalapudi D, Basu S N, Ludvig K F Jr. and Moustakas T D, 1998 *J. Appl. Phys*. **84** 1389.

[9] Moon Y-T, Kim D-J, Song K-M, Coi C-J, Han S-H, Seong T-Y and Park S-J 2001 *J. Appl. Plys*. **89** 6514.

[10] Ho I H and Stringfellow G B 1996 *Appl. Phys. Lett.* **69** 2701.

[11] Karpov S Yu 1998 *J. Nitride Semicond. Res*. **3** 16.

[12] Osamura K, Nakajima K and Murakami Y 1972 *Solid State Commun*. **11** 617.

[13] Lin Y-S, Ma K-J, Hsu C, Chung Y-Y, Liu C-W, Feng S-W, Cheng Y-C, Mao M-H, Yang C C, Chuang H-W, Kuo C-T, Tsang J-S and Weirich T E 2002 *Appl. Phys. Lett*. **80** 2571.

[14] Feng S-W, Chung Y-Y, Liu C-W, Cheng Y-C, Yang C C, Mao M-H, Lin Y-S, Ma K-J, Chyi J-I 2002 *Appl. Phys. Lett*. **80** 4375.

[15] Chichibu S, Azuhata T, Sota T and Nakamura S 1997 *Appl. Phys. Lett.* **70** 2822.

[16] Chichibu S, Sota T, Wada K and Nakamura S 1998 *J. Vac. Sci. Technol*. B **16** 2204.

[17] O'Donnell K P, Martin R W and Middleton P G 1999 *Phys. Rev. Lett*. **82** 237.

[18] Cho Y-H, Schmidt T J, Bidnyk S, Gainer G H, Song J J, Keller S, Mishra U K and DenBaars S P 2000 *Phys. Rev.* B **61** 7571.
[19] Kent P R and Zunger A 2001 *Appl. Phys. Lett*. **79** 1997.
[20] Narukawa Y, Kawakami Y, Fujita S, and Nakamura S, 1999 *Phys. Rev*. B **59** 10283.
[21] Baranovskii S D, Eichmann R and Thomas P 1998 *Phys. Rev. B* **58** 13081.
[22] Kazlauskas K, Tamulaitis G, Zukauskas A, Khan M A, Yang J W, Zhang J, Simin G, Shur M S and Gaska R 2003 *Appl. Phys. Lett*. **83** 3722.
[23] Minsky M S, Watanabe S and Yamada N, 2002 *J. Appl. Phys*. **91** 5176.
[24] Bernardini F and Fiorentini V 1998 *Phys. Rev. B* **58** 15292.
[25] Lefebvre P, Morel A, Gallart M, Taliercio T, Allègre J, Gil B, Mathieu H, Damilano B, Grandjean N and Massies J 2001 *Appl. Phys. Lett*. **78** 1252.
[26] Chow W W, Amano H, Takeuchi T and Han J 1999 *Appl. Phys. Lett*. **75** 244.
[27] Böttcher T, Einfeldt S, Kirchner V, Figge S, Heinke H, Hommel D, Selke H and Ryder P L 1998 *Appl. Phys. Lett*. **73**, 3232.
[28] Shimizu M, Kwaguchi Y, Hiramatsu K and Sawaki N 1997 *Solid-state electron*. **41** 145.

2.2. PHOTOLUMINESCENCE LINE WIDTH ANALYSIS IN InGaN MULTIPLE QUANTUM WELLS USING MONTE CARLO SIMULATION OF EXCITON HOPPING

By
A. Zukauskas, K. Kazlauskas, G. Tamulaitis, P. Pobedinskas, S. Jursėnas
Institute of Materials Science and Applied Research, Vilnius University, Vilnius, Lithuania
M. Springis, I. Tale
Institute of Solid State Physics University of Latvia, Riga, Latvia
Yung-Chen Cheng, Hsiang-Cheng Wang, Chi-Feng Huang, and C. C. Yang
Graduate Institute of Electro-Optical Engineering and Department of Electrical Engineering, National Taiwan University 1, Roosevelt Road, Sec. 4, Taipei, Taiwan, R.O.C

Abstract
Temperature dependence of the photoluminescence (PL) line width in thin $In_{0.2}Ga_{0.8}N$/GaN multiple quantum wells (MQWs) was analyzed using Monte Carlo simulation of exciton hopping. The dependence was shown to reveal a crossover from nonthermalized to thermalized exciton energy distribution at 150 K and fluctuations of the band potential with additional broadening that we attributed to formation of In-rich regions. Based on the fitting procedure, band potential fluctuations within In-rich regions (31 meV), dispersion of the average exciton energy in different In-rich regions (29 meV) and a Bose-Einstein-like temperature dependence of the exciton energy in the wells were extracted.

2.2.1. Introduction

InGaN/GaN MQWs are the key components of many commercial devices emitting green, blue, near UV, and white light. It is generally accepted that inhomogeneous distribution of indium facilitates high quantum efficiency of InGaN-based light emitting devices [1]. Formation of In-rich regions in InGaN is proved by high-resolution microscopy and X-ray microanalysis [2,3], spatially resolved cathodoluminescence [4], and near field optical microscopy [5,6]. However despite a tremendous commercial success, InGaN remains a puzzling material mainly because of incompletely unveiled link of its intricate structure with electronic properties. This hinders further improvement of the device performance, which is the key issue for deeper penetration of semiconductor optoelectronics into the lumen market.

PL provides with a deep but experimentally unsophisticated insight into carrier and exciton dynamics in semiconductors. In particular, in group-III nitride alloys and relevant quantum wells, photoluminescence is known to exhibit an anomalous temperature behavior of the peak position (S-shaped dependence) and line width (W-shaped dependence) [7-13] indicating an intricate character of carrier/exciton motion through localized states (hopping) [14-16]. Recently this anomalous behavior received more attention in terms of theoretical modeling of the hopping process. In particular, a double-scaled character of the potential profile was unveiled and parameters of band potential fluctuations were estimated in bulk quaternary AlInGaN alloy by using the Monte Carlo simulation of exciton hopping [17].

We apply the Monte Carlo simulation of exciton hopping for analysis of the PL line width temperature dependence in InGaN MQWs.

2.2.2. Experimental

Narrow quantum wells were chosen for investigation to minimize distortions of the PL spectra due to quantum-confined Stark effect caused by the built-in piezoelectric and spontaneous-polarization fields. The sample was grown by metal-organic chemical vapor

deposition over a sapphire substrate and consisted of five 2-nm thick $In_{0.22}Ga_{0.78}N$ quantum wells separated by 9-nm thick GaN barriers deposited on a 2.5 μm thick GaN buffer layer.

A continuous-wave He-Cd laser emitting at 325 nm was used for excitation. The luminescence signal was dispersed by a double monochromator (Jobin Yvon HRD-1) and recorded by using a photomultiplier (Hamamatsu R1463P) in the photon counting regime. A closed-cycle helium refrigerator was employed to perform the measurements at temperatures down to 10 K. To avoid distortions of the PL line shape due to Fabri-Perrot interference caused by multiple reflections of light between the substrate and sample surface (that are ~2.5 μm apart), we collected the PL signal propagating through the transparent substrate that was frosted to randomize the angles of the escaping photons.

The PL excitation spectra were measured by using monochromatized light of tungsten lamp as an excitation source. The measurements were carried out at fixed temperatures down to 8 K by using a closed-cycle helium cryosystem.

The mean exciton position in the samples was determined by using photoreflectance technique. A DSP lock-in amplifier *Signal Recovery* 7265 was employed in photoreflectance measurements. Reflection of collimated light of a tungsten-halogen lamp was measured under influence of radiation of He–Cd laser (325 nm) modulated by mechanical chopper, which was driven by the lock-in amplifier. The photoreflectance spectra were analysed by using standard procedures [18].

2.2.3. Double-scaled potential in InGaN multipple quantum wells

The near-band-edge PL spectra measured at different temperatures are presented in Fig. 2.2.1. The spectra contain a single band with two humps on the low-energy slope separated by approximately 90 meV. We attribute these features to direct and longitudinal-optical-phonon replicated recombination of localized excitons, respectively. The PL intensity maintains an almost stable value below 50 K and decreases at elevated temperatures, most probably, due to enhanced influence of nonradiative recombination.

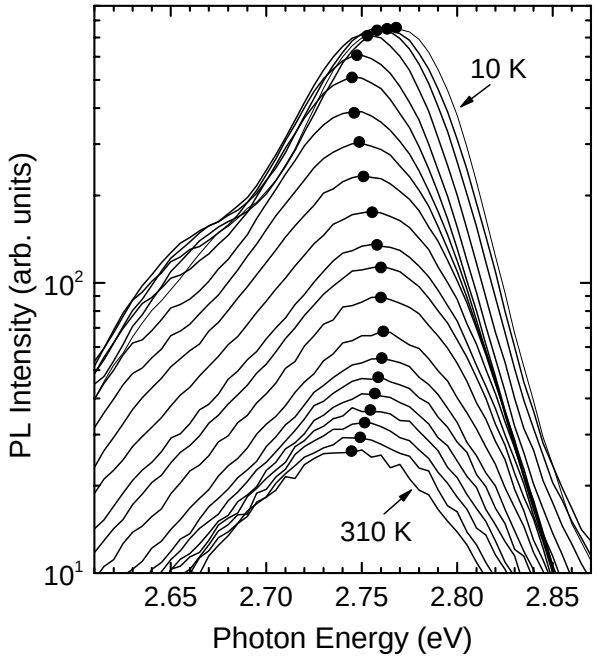

Fig. 2.2.1. Evolution of the PL spectra with temperature in InGaN/GaN MQWs. The temperature is incremented by 15 K starting with 10 K (the uppermost spectrum) and ending with 310 K (the lowermost spectrum). The band peak positions are indicated by dots.

The PL band peak position is highlighted by dots in Fig. 2.2.1. The peak exhibits a well-established S-shaped temperature behavior [7–9]: it slightly redhifts in the range from 10 K to 50 K, then blueshifs up to 150 K, and redshifts again afterwards. Points in Fig. 2 show a W-shaped temperature dependence of the full width at half maximum (FWHM) of the PL band

with a characteristic kink at about 150 K. The S-shaped temperature behavior of the PL band peak position and the W-shaped temperature behavior of the line width are known to be a signature of exciton hopping over randomly dispersed localized states with a crossover from a nonthermalized to a thermalized distribution function of the excitons [17]. Under appropriate selection of the electronic potential profile, exciton hopping is able to quantitatively account for the PL line width and the Stokes shift of the PL band in respect of the average exciton energy in group-III nitride alloys as revealed by our recent three-dimensional (3D) Monte Carlo simulation in AlInGaN bulk-like layers [17]. Here we applied a Monte Carlo simulation routine for exciton hopping in 2D regime and demonstrated that the potential profile can be described based only on the experimental temperature dependence of the PL line width. Simultaneously, we deduced the Stokes shift of the PL band and reconstructed the temperature dependence of the average exciton energy in our MQW structure using the measured PL peak positions.

The observed temperature behavior of the PL line width was simulated by using a 2D Monte Carlo procedure with the Miller-Abrahams rate for phonon-assisted exciton tunneling between the initial and final states *i* and *j* with the energies E_i and E_j, respectively,

$$\nu_{i\to j} = \nu_0 \exp\left(-\frac{2r_{ij}}{\alpha} - \frac{E_j - E_i + \left|E_j - E_i\right|}{2k_B T} \right). \qquad (2.2.1)$$

Here r_{ij} is the distance between the states, α is the decay length of the exciton wave function, and ν_0 is the attempt-to-escape frequency. Hopping was simulated over a randomly generated set of localized states with the sheet density *N* and localization energies dispersed in accordance with a Gaussian distribution with the central position at exciton energy and the dispersion parameter (the energy scale of the band potential profile fluctuations) σ. For each excited exciton, the hopping process terminates by recombination with the probability τ_0^{-1} and the energy of the localized state where the recombination has taken place from is scored to the emission spectrum $S_0(h\nu)$.

Fitting of the temperature dependence of the width of the simulated PL band to the experimental results reveals the important peculiarities as follows. In the initial 10 K to 150 K region, the variation of the line width is due to thermal enhancement of exciton hopping within nonthermalized energy distribution and the shape of the dependence is basically a function of the spatial (the product $N\alpha^2$) and temporal (the product $\nu_0\tau_0$) parameters of the hopping process. The kink in the temperature dependence of the line width at about 150 K represents a crossover from a nonthermalized to thermalized energy distribution of excitons and the crossover temperature is related mainly with the energy scale of the band potential profile fluctuations σ. Finally, an almost constant line width right above the crossover temperature (150–180 K) indicates an occurrence of a thermalized exciton energy distribution and is determined by the energy scale σ and additional inhomogeneous broadening Γ that results in a modified emission spectrum

$$S(h\nu) = \int S_0(h\nu')\, G(\Gamma, h\nu - h\nu')\, d\, h\nu', \qquad (2.2.2)$$

where $G(\Gamma, h\nu)$ is a standard Gaussian function with dispersion Γ. The further increase of the line width above 180 K is attributed to the influence of delocalized excitons that are not taken into account in the model used.

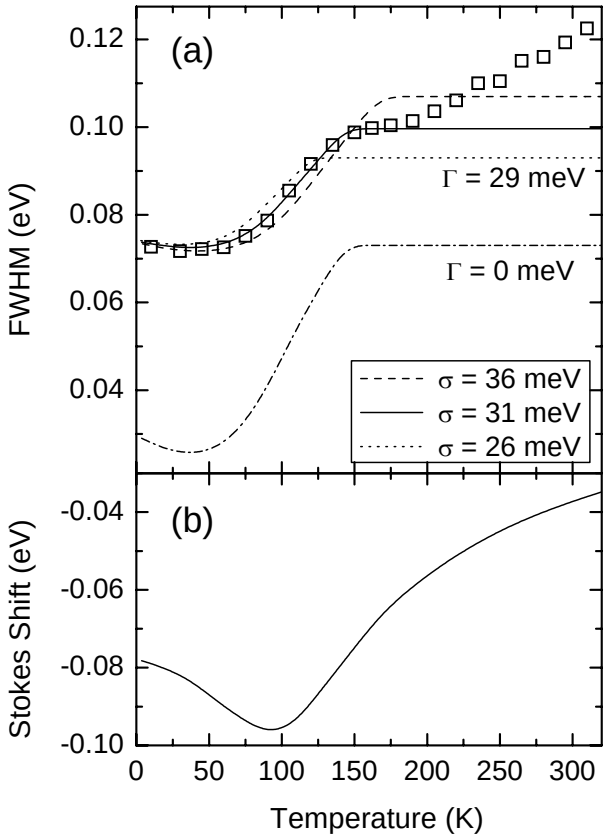

Fig. 2.2.2
(a) Temperature dependence of the full width at half maximum of the photoluminescence band in 2-nm InGaN/GaN MQWs. Points depict experimental data; dashed, dotted and solid lines show results of Monte Carlo simulation of exciton hopping for different scales of random potential fluctuations σ (indicated) with the inhomogeneous broadening Γ of 29 meV taken into account; dashed-dotted line represents results for $\sigma = 31$ meV and $\Gamma = 0$.
(b) Temperature dependence of the Stokes shift of the PL band peak position in respect of the average exciton energy corresponding to the best-fitted line width dependence.

Solid line in Fig. 2.2.2a represents the result of the best fit obtained for the following values of the parameters: $N\alpha^2 = 1$, $\nu_0\tau_0 = 3\times10^5$, $\sigma = 31$ meV, and $\Gamma = 29$ meV. Dashed and dotted lines demonstrate sensitivity of the simulation results in respect of the hopping energy scale σ and a dashed-dotted line shows the simulated dependence without inhomogeneous broadening.

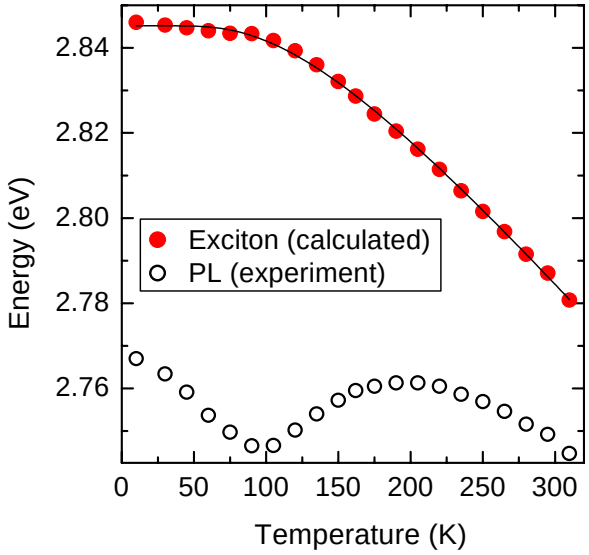

Fig. 2.2.3. Measured photoluminescence band peak position (open dots) and the reconstructed average exciton energy (solid dots) as a function of temperature. Solid line represents the best fit by using the Bose-Einstein-like formula.

Our simulation reveals a double-scaled band potential profile in InGaN quantum wells similar to that deduced in AlInGaN bulk-like layers [17]. Such a band potential profile implies

hopping of excitons within isolated In-rich regions with the localized-state energy dispersion σ, whereas the average exciton energy is different in each In-rich region and is dispersed over the scale Γ. We attribute the dispersion Γ to different average indium content within the In-rich regions. Moreover in quantum wells, both the energy scale σ and the inhomogeneous broadening Γ can be increased by well-width fluctuations that modulate quantum confinement energy.

Figure 2.2.2b depicts the temperature behavior of the Stokes shift deduced from the peak position of the simulated spectra. Based on this data and the measured peak positions of the PL band (open points in Fig. 2.2.3), the temperature dependence of the average exciton energy was reconstructed (filled points in Fig. 2.2.3). The dependence is fairly well described by the Bose-Einstein-like expression

$$E(T) = E(0) - \frac{\lambda}{\exp(\theta/T) - 1} \tag{2.2.3}$$

with the best-fit parameters $\lambda =$ 0.154 eV, $\theta =$ 379 K, and $E(0) =$ 2.8452 eV. Although obtained in a rather indirect way, this result provides supplementary data on characterization of thin quantum wells with relatively high In molar fraction, where the exciton energy is difficult to precisely measure (e.g. using absorption, reflection, or photoluminescence excitation spectroscopy) because of low optical density and considerable broadening of the spectra.

2.2.4. Potential profile as a function of indium content in InGaN multipple quantum wells

To study the influence of indium content on the double-scaled potential profile in InGaN quantum wells revealed in 2.2.3, we measured the temperature evolution of PL spectra in three samples containing InGaN/GaN MQWs with different indium content in the well material. The In molar fraction was about 22%, 25%, and 27% in samples 2, 4, and 3, respectively. The spectra are presented in Fig. 2.2.4.

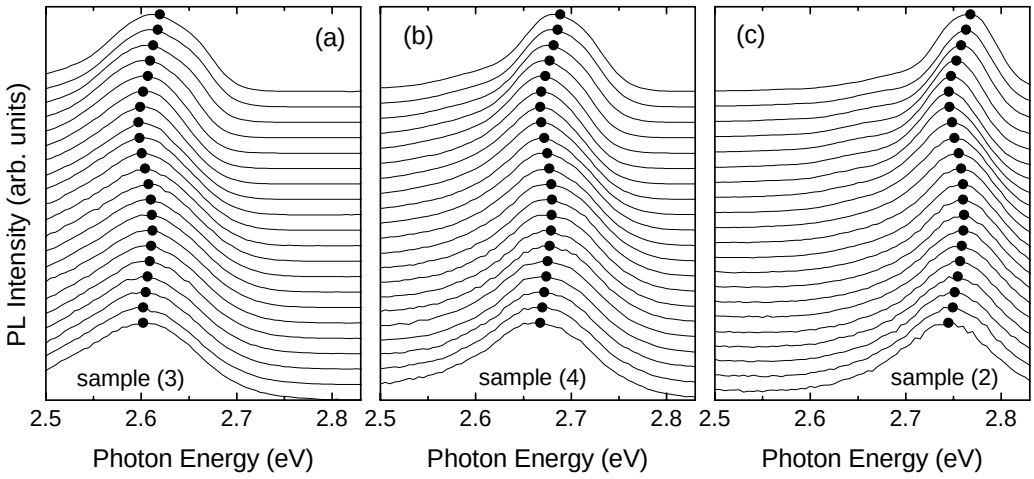

Fig. 2.2.4. Photoluminescence spectra of InGaN/GaN MQW samples 3 (a), 4 (b), and 2 (c), as a function of temperature in the range from 15 K to 310 K. Spectra are arbitrarily shifted along the vertical axis. The points indicate PL peak energy.

The black dots in Fig. 2.2.4 indicate the band peak positions for every spectrum and reveal an S-shaped temperature dependence of the peak position for all three samples. The absolute position of the PL peaks at fixed temperature redshifts with increasing indium content,

however, this shift can also be caused by different influence of carrier/exciton localization as well as by modification of built-in electric fields. To make use of the PL data for quantitative description of nonequilibrium carriers in the MQWs under study, exciton position in the samples is necessary as a reference. Thus, we measured photoluminescence excitation (PLE) spectra, which are often used to characterize the band gap of a semiconductor.

The PLE spectra at different temperatures are presented in Fig. 2.2.5. The spectra have a structure at approximately 3.4 eV, which is obviously related with absorption of GaN in barriers and buffer layer. The structure redshifts with increasing temperature, as should be expected due to band gap shrinkage usually described in GaN by the common Varshni formula. The PLE spectra also contain a long-wavelength tail, which is obviously related to excitation of InGaN in the wells. Unfortunately, this tail smoothly extends down to the region of the PL band and has no distinct featured useful for quantitative characterization of the absorption edge.

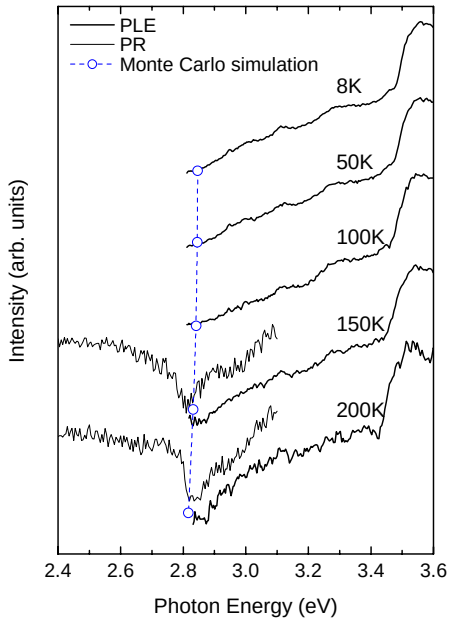

Fig. 2.2.5. Photoluminescence excitation (bold lines) and photoreflectance spectra (thin lines) of sample 2 at different temperatures. Circles indicate exciton energy estimated from Monte Carlo simulation.

In contrast, the photoreflectance spectra (depicted by thin lines in Fig. 2.2.5) have a typical excitonic feature. In spite of considerable inhomogeneous broadening, the structure is sharp enough to apply fitting with the calculated photoreflectance spectrum and to retrieve the exciton energy, which is used as one of the fitting parameters. The accuracy of the fitting and exciton energy determination is demonstrated by error bars at several temperatures for sample 2 in Fig. 2.2.6.

Fig. 2.2.6 depicts also the PL spectra measured at the same temperatures as the PR spectra. A considerable Stokes shift is evident and may be interpreted by localization of the photoexcited carriers/excitons.

To further describe quantitatively the energy spectrum for carriers in the three samples we applied the Monte Carlo simulation described in 2.2.4. The best-fit curves describing the temperature dependence of the FWHM of the PL band are presented together with the experimental data for the three samples under study in Fig. 2.2.7. The fitting was performed with parameters $N\alpha^2 = 1$, $\nu_0\tau_0 = 3\times10^5$.

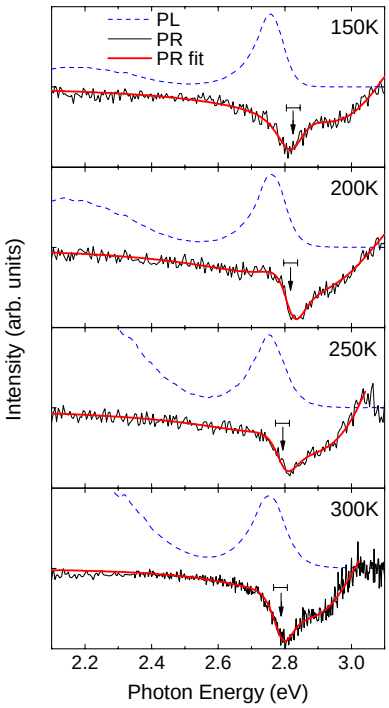

Fig. 2.2.6. Photoluminescence and photoreflectance spectra of sample 2 at different temperatures. The exciton transition energy (indicated by an arrow) within an uncertainty (indicated by an error bar) was determined by fitting experimental PR data (thin solid line) with a theory (thick solid line). PL spectra are indicated by dashed lines.

The localized-state energy dispersion σ for hopping of excitons within isolated In-rich regions slightly increase with increasing In content from 31 eV in sample 2 to 33 meV in sample 4 to 38 meV in sample 3. Meanwhile, the dispersion Γ due to different average indium content within the In-rich regions shows a stronger increase with increasing average indium content in the quantum wells. Its estimated value equals 29, 39, and 47 meV in the samples 2, 3, and 4, respectively.

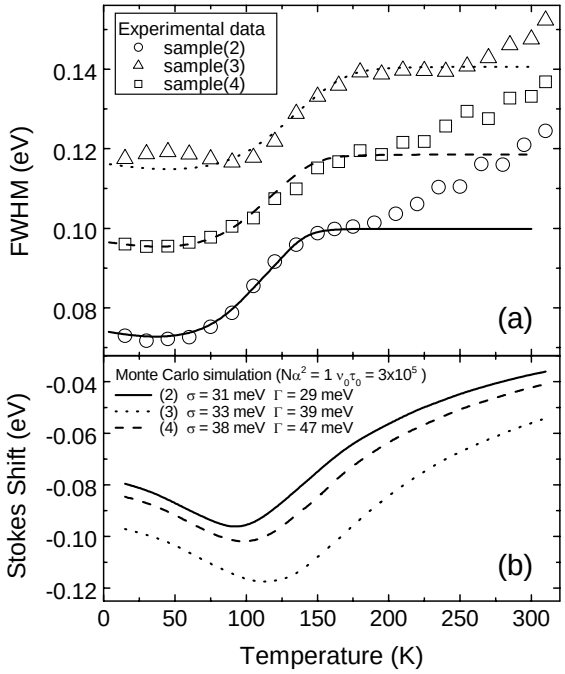

Fig. 2.2.7. (a) Temperature dependence of the full width at half maximum (FWHM) of PL band in three InGaN/GaN MQW samples with different indium content. Circles, triangles and squares depict experimental data for samples 2, 3 and 4, respectively; lines show results of Monte Carlo simulation of exciton hopping for different scales of random potential fluctuation σ (indicated) and inhomogeneous broadening Γ (indicated) taken into account.

(b) Temperature dependence of the Stokes shift of the PL band peak position in respect of the average exciton energy corresponding to the best-fitted line width temperature dependence for samples 2, 3 and 4.

As demonstrated in Fig. 2.2.7, the Monte Carlo simulation provides satisfactory description of the FWHM dependence on temperature up to the plateau, which extends

approximately to 180 K in the sample with the lowest In content and to 250 K in the sample with the highest In content. The plateau corresponds to the situation when the excitons are thermalized over the localized states within the In-rich region, while the subsequent increase of FWHM with the further increase of temperature in caused by homogeneous broadening due to thermalization of the carriers through the extended states. Comparison of the three samples demonstrates that the larger dispersion of the localized states energies σ corresponds to a broader plateau in the temperature dependence of the FWHM and to a higher temperature of the crossover from the inhomogeneous to homogeneous broadening of the PL band.

The Monte Carlo simulation enabled us to reconstruct the temperature dependence of the exciton position in all three samples under study (see Fig. 2.2.8). The dependence follows the Bose-Einstein-like expression (2.2.3) with parameters indicated in Fig. 2.2.8. Filled points with error bars in Fig. 2.2.8 indicate exciton energies as determined by using the photoreflectance spectra. It is evident that the shift of the exciton energy estimated from PR spectra coincides within the experimental error with the shift recovered by using the Monte Carlo simulation. Taking into account the large inhomogeneous broadening observed in the samples under study, the coincidence is satisfactorily and provides additional proof of applicability of the Monte Carlo simulation procedure, which we developed to characterize the system of nonequilibrium carriers/excitons in InGaN.

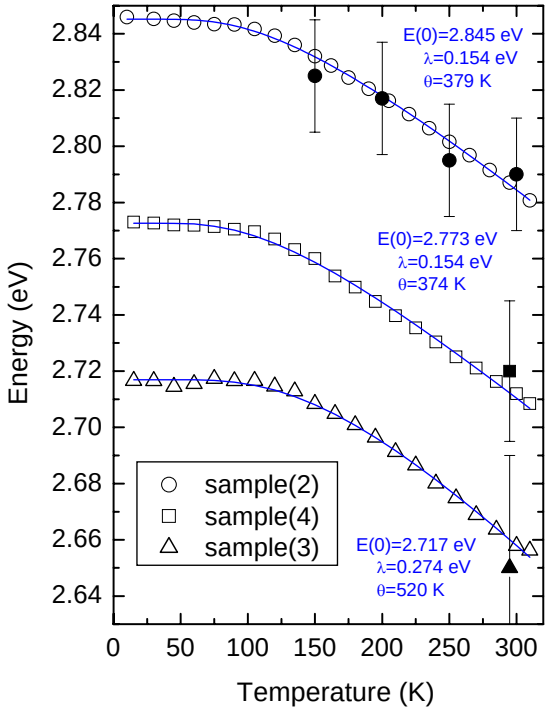

Fig. 2.2.8. Temperature dependence of the reconstructed average exciton energy for sample 2 (open circles), 3 (open triangles) and 4 (open squares). Lines represent the best fit obtained with Bose-Einstein-like expression. The fitting coefficients are shown above each fitting curve. Filled points with error bars indicate exciton energies as determined by photoreflectance measurements.

2.2.5. Conclusions

In conclusion, we have demonstrated an analysis of temperature behavior of the PL line width in InGaN/GaN MQWs by using Monte Carlo simulation of exciton hopping. The simulation revealed band potential fluctuations within individual In-rich regions (31 meV), dispersion of the average exciton energy in different In-rich regions (29 meV), and a Bose-Einstein-like temperature dependence of the average exciton energy in the wells. With increasing In content from about 22% to 27%, the localized-state energy dispersion σ for hopping of excitons within isolated In-rich regions increase from 31 eV to 38 meV. Meanwhile, the dispersion Γ due to different average indium content within the In-rich regions changes from 29 to 47 meV in the same samples, respectively. Our results suggest that excitons migrate and radiatively recombine within isolated In-rich regions with the average band potential lower than that in

the surrounding InGaN matrix. Increased In molar fraction results mainly in an increase in dispersion of the average energy of In-rich regions, meanwhile the band potential fluctuations within the regions increase to a smaller extent.

References

[1] S. Chichibu, T. Sota, K. Wada, S. Nakamura, J. Vac. Sci. Technol. B **16**, 2204 (1998).
[2] Y. Narukawa, Y. Kawakami, M. Funato, S. Fujita, S. Fujita, and S. Nakamura, Appl. Phys. Lett. **70**, 981 (1997).
[3] Y. S. Lin, K. J. Ma, C. Hsu, S. W. Feng, Y. C. Cheng, C. C. Liao, C. C. Yang, C. C. Chou, C. M. Lee, and J. I. Chyi, Appl. Phys. Lett. **77**, 2988 (2000).
[4] S. Chichibu, K. Wada, and S. Nakamura, Appl. Phys. Lett. **71**, 2346 (1997).
[5] A. Vertikov, A. V. Nurmikko, K. Doverspike, G. Bulman, J. Edmond, Appl. Phys. Lett. **73**, 493 (1998).
[6] J. Kim, K. Samiee, J. O. White, J.-M. Myoung, and K. Kim, Appl. Phys. Lett. **80,** 989 (2002).
[7] Y.-H. Cho, G. H. Gainer, J. B. Lam, J. J. Song, W. Yang, and W. Jhe, MRS Internet J. Nitride Semicond. Res. **5S1**, W11.57 (2000).
[8] P. G. Eliseev, P. Perlin, J. Lee, and M. Osinski, Appl. Phys. Lett. **71**, 569 (1997).
[9] Y.-H. Cho, T. J. Schmidt, S. Bidnyk, G. H. Gainer, J. J. Song, S. Keller, U. K. Mishra, and S. P. DenBaars, Phys. Rev. B **61**, 7571 (2000).
[10] J. Li, K. B. Nam, J. Y. Lin, and H. X. Jiang, Appl. Phys. Lett. **79**, 3245 (2001).
[11] T. Wang, Y. H. Liu, Y. B. Lee, J. P. Ao, J. Bai, and S. Sakai, Appl. Phys. Lett **81**, 2508 (2002).
[12] H. Hirayama, A. Kinoshita, T. Yamabi, Y. Enomoto, A. Hirata, T. Araki, Y. Nanishi, and Y. Aoyagi, Appl. Phys. Lett. **80**, 207 (2002).
[13] K. Kazlauskas, G. Tamulaitis, A. Žukauskas, M. A. Khan, J. W. Yang, J. Zhang, E. Kuokstis, G. Simin, M. S. Shur, and R. Gaska, Appl. Phys. Lett. **82**, 4501 (2003).
[14] D. Monroe, Phys. Rev. Lett. **54**, 146 (1985).
[15] S. A. Tarasenko, A. A. Kiselev, E. L. Ivchenko, A. Dinger, M. Baldauf, C. Klingshirn, H. Kalt, S. D. Baranovskii, R. Eichmann, and P. Thomas, Semicond. Sci. Technol. **16**, 486 (2001).
[16] S. D. Baranovskii, R. Eichmann, and P. Thomas, Phys. Rev. B **58**, 13081, (1998).
[17] K. Kazlauskas, G. Tamulaitis, A. Žukauskas, M. A. Khan, J. W. Yang, J. Zhang, G. Simin, M. S. Shur, and R. Gaska, Appl. Phys. Lett. **83**, 3722 (2003).
[18] F. H. Pollak and H. Shen, Mater. Sci. Engr. R **10**, 275 (1993).

2.3. QUANTUM-CONFINED STARK EFFECT AND LOCALIZATION OF CARRIERS SELECTIVELY PHOTOEXCITED INTO InGaN QUANTUM WELLS

By
G. Tamulaitis, K. Kazlauskas, J. Mickevičius, A. Žukauskas
Institute of Materials Science and Applied Research, Vilnius University, Vilnius, Lithuania
Yung-Chen Cheng, Hsiang-Cheng Wang, Chi-Feng Huang, and C. C. Yang
Graduate Institute of Electro-Optical Engineering and Department of Electrical Engineering, National Taiwan University 1, Roosevelt Road, Sec. 4,
Taipei, Taiwan, R.O.C

Abstract
Carrier localization and well tilting effects were studied in multiple quantum wells (MQW) containing $In_{0.15}Ga_{0.85}N$ well layers of different thickness ranging from 2 to 4 nm by using photoluminescence (PL) excited by photons of different energy in a wide range of excitation power density. Comparison of experimentally obtained PL spectra with calculations of the lowest optical transitions with screening effects taken into account enabled us to partially separate contributions of the well tilting and carrier localization in the redshift of the PL band. The dynamics of the PL band shift with increasing carrier density generated either in quantum wells or both in the wells and GaN barrier layers was shown to be in consistence with an assumption that the In-rich regions serving for accumulation of photoexcited carriers are formed on the well-barrier interface and extend to the barrier layer.

2.3.1. Introduction

Compound InGaN is already established as the material of choice in many commercial light-emitting devices emitting in green and blue regions. Many results on spatially resolved analysis [1–6] evidence inhomogeneous distribution of indium in this ternary compound. This inhomogeneity results in localization of nonequilibrium carriers and, as generally believed, enhances performance of InGaN-based light emitting devices [7]. In multiple quantum wells (MQW), which are usually used in InGaN-based devices, the efficiency of light emission is, however, inhibited by quantum well tilting due to quantum confined Stark effect. The effect is caused by built-in electric fields due to spontaneous and piezoelectric polarization at well-barrier interfaces and results in spatial separation of electrons and holes. Both the localization and the well tilting redshift the energies of optical transitions. On the other hand, increasing density of nonequilibrium carriers results in filling of the localized states as well as in screening of the built-in electric field. Both these effects blueshift the energies of optical transitions. Thus, it is difficult to reveal the contribution of the localization and the well tilting by using luminescence spectroscopy that is one of the most informative techniques to study nonequilibrium carriers and is directly related with light emission, which is of interest for many applications.

Comparison of measured temperature dependence of PL characteristics with results of Monte Carlo simulation of exciton hopping led us to a conclusion that the excitons in nitride compounds experience a double-scaled potential profile [8]. The nonequilibrium carriers/excitons accumulate in In-rich regions where the average potential is lower than that in surrounding matrix with lower In content and move by hopping through localized states dispersed at smaller energy scale due to random potential fluctuations. In chapter 2.2, we demonstrated that in $In_{0.2}Ga_{0.8}N$/GaN MQWs the energy dispersion due to random potential

fluctuations is approximately 30 meV, while the average potential within the In-rich regions is dispersed within ~70 meV.

The study of InGaN MQWs by using high resolution transmission electron microscopy (HRTEM) revealed that the In-rich regions have a tendency to form on the well-barrier interface and to extend into the barrier layer when the average In content is increased in the range of 15%-20% [5].

We studied localization of nonequilibrium carriers and well tilting due to built-in electric field in a set of samples containing InGaN MQWs of different thickness. To get a new insight into the problem, we investigated the PL spectra evolution under increasing excitation intensity for two photon energies of the excitation light. The first photon energy was sufficient to selectively excite InGaN in the quantum well but was too small for excitation of GaN barriers. The second photon energy was high enough to excite both wells and barriers.

2.3.2. Experimental

The MQWs under study were grown by metalorganic chemical vapor deposition (MOCVD) on sapphire substrate covered by 30 nm buffer layer and a 2.3 μm thick layer of n-GaN. The samples consisted of five $In_{0.15}Ga_{0.85}N$ quantum wells separated by 10 nm-thick GaN barriers. A set of 5 samples with different well widths of 2.0, 2.5, 3.0, 3.5, and 4.0 nm were grown in otherwise identical conditions.

A cw He-Cd laser emitting at 325 nm was used as a low-power excitation source. High excitation power densities were applied under pulsed excitation by a dye laser pumped by the 3rd harmonic of YAG:Nd laser radiation. Pulse duration of 10 ns ensured quasi-steady-state excitation conditions. Two excitation photon energies were selected. Photons with energy $h\nu_{exc} = 3.255$ eV, which is below the bandgap of GaN, excited carriers only in the quantum well material, while both well and barriers were excited by photons with $h\nu_{exc} = 3.625$ eV.

The PL spectra were measured by using the Jobin Yvon spectrometer HRD-1 and a photomultiplier. CW spectra were recorded in photon counting mode while a boxcar integrator was used in experiments with pulsed excitation.

2.3.3. Experimental results

The PL spectra under cw excitation are illustrated in Fig. 2.3.1a. The PL band blueshifts with decreasing well width as depicted by dots in Fig. 2.3.1b.

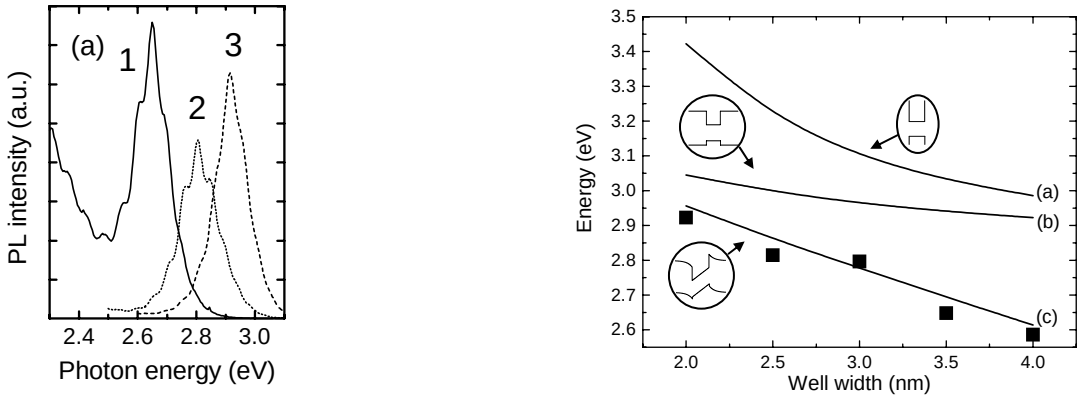

Fig. 2.3.1. Photoluminescence spectra of InGaN MQW structures with well width of 3.5 (1), 2.5 (2), and 2.0 nm (3) under CW excitation (a), and well width dependence of PL peak positions observed experimentally (points) and calculated by using models of quantum well with infinitive barriers, finite barriers, and with the quantum-confined Stark effect taken into account (as indicated by inserts) (b).

The PL intensity does not decrease with increasing well width, as might be expected due to increasing spatial separation of electrons and holes caused by quantum-confined Stark effect. This is an indication that other effect, most probably, carrier localization is also important for emission efficiency in the samples under study. A broad band of yellow luminescence is also observed, and its intensity is higher in samples with higher well widths.

The dynamics of the PL spectra with increasing excitation power density under pulsed excitation for two samples with 2 nm and 4 nm wide quantum wells is presented in Fig. 2.3.2. The spectra presented in Fig. 2.3.2(a) and (c) were taken under excitation by photons (3.625 eV) absorbed both in the well and barrier layers, the spectra in Fig. 2.3.2(b) and (d) were measured under selective excitation of the well material with 3.255 eV energy photons. The PL spectrum in the samples with narrow MQWs is dominated by a single band, while an additional band in the blue side from the main band emerges in the spectra with increasing well width. The second band is better pronounced under selective excitation of the wells (see Fig. 2.3.2d). The band peaked at ~3.42 eV is caused by the photoexcited carriers generated in the GaN barrier layers and recombining before their relaxation into the wells.

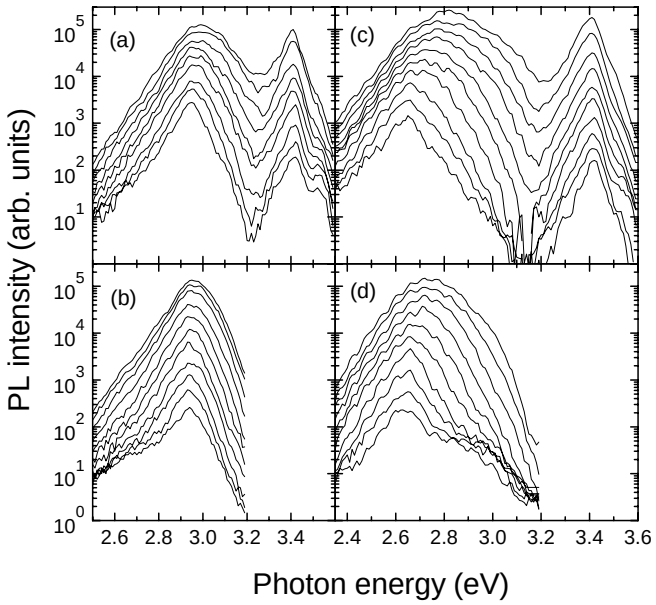

Fig. 2.3.2. PL spectra of InGaN MQW with well width of 2.0 nm (a), (b) and 4.0 nm (c), (d) at excitation photon energy of 3.625 eV (a), (c) ir 3.255 eV (b), (d) measured at increasing excitation power density

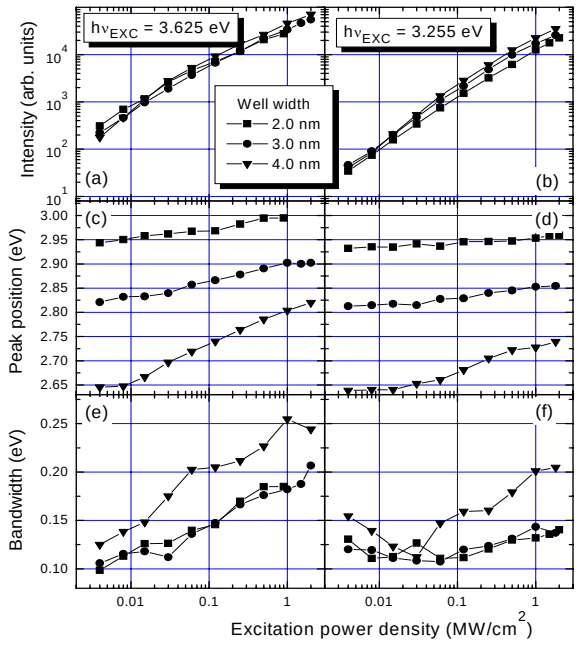

Fig. 2.3.3. Excitation power density dependence of spectrally integrated PL intensity (a) and (b), PL band peak position (c) and (d), and bandwidth (e) and (f) in quantum wells of 2 (squares), 3 (dots), and 4 nm (triangles). Excitation photon energy was 3.625 eV (a), (c), (e) and 3.255 eV (b), (d), (f).

The parameters of the main PL band as a function of excitation power density are summarized in Fig. 2.3.3. The PL intensity dependence on the excitation power density is close to linear in all samples and under both selective and unselective excitation within the range of 3 orders of magnitude up to 2 MW/cm^2 that is close to the threshold of permanent surface damage. Since the excitation by the light effectively absorbed in the barrier layers ($h\nu$ = 3.625 eV) results in higher carrier density than in the case of selective excitation of the quantum wells by 3.255 eV photons at the same pump intensity, we normalized the effective power density by using PL intensity dependence on the excitation power density. The excitation power density in Fig. 2.3.3-2.3.5 are presented in arbitrary units corresponding to the same PL intensity for both excitation photon energies.

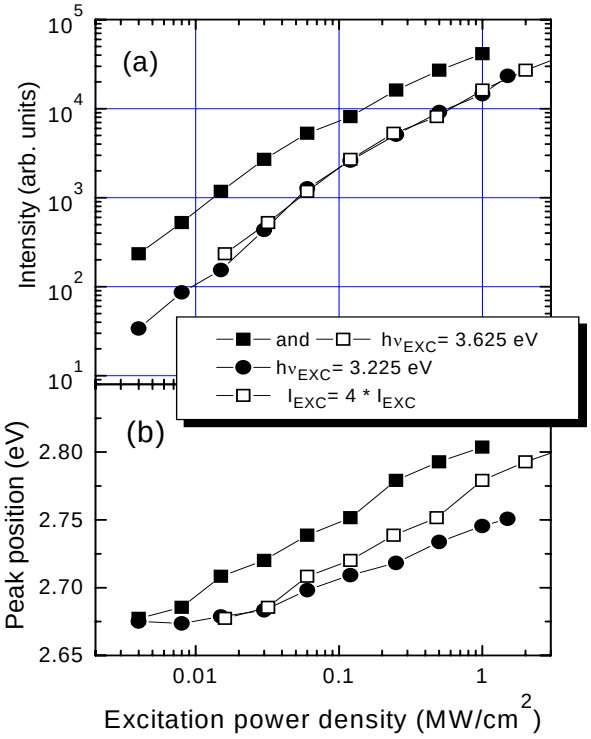

Fig. 2.3.4. Excitation power density dependence of spectrally integrated PL intensity (a) and PL band peak position (b) under excitation at 3.255 eV (squares) and 3.625 eV (dots) in InGaN MQWs with well width of 3.5 nm.

A blueshift and band broadening with increasing pump intensity is observed and the effects are stronger in broader quantum wells. The dependencies measured for two excitation power densities in the sample containing 3.5 nm wide quantum wells are compared in Fig. 2.3.4. The blueshift with increasing excitation power proceeds obviously faster when the barriers are excited (at $h\nu_{exc}$ = 3.625 eV). This feature is observed in MQWs with different well widths.

The PL band blueshift as a function of excitation power density is depicted for 3 well widths by points in Fig. 2.3.5. There, points corresponding to CW pulsed excitation are presented together to cover a wide power density range of 9 orders of magnitude. The blueshift is more pronounced in MQWs with broader wells.

2.3.4. Calculations

The experimentally observed blueshift of the PL band with increasing excitation power density is possibly caused by i) population of localized states, and ii) screening of the built-in electric field by the photoexcited cariers. The two effects have the same sign and are difficult to distinguish experimentally. Thus, we complemented the experimental results by theoretical

calculations of the energy of the lowest optical transition and its dynamics due to screening effect.

To calculate the energies of optical transitions responsible for PL we used three models. The first model of quantum wells with infinite barriers gave PL peak positions considerably shifted in respect to those observed experimentally (see Fig. 2.3.1b). Introduction of finite barrier heights (0.535 eV and 0.045 eV band offsets for electrons and holes, respectively[9]) gave smaller but still unacceptable deviation from experimental results (Fig. 2.3.1b, curve (b)). A satisfactory fit was achieved with the well tilting due to built-in electric field taken into account (as represented by curve (c) in Fig. 2.3.1b for the value of the built-in electric field of 1.7 MV/cm). The calculations according to the letter two models were based on solution of the Schroedinger equation and accomplished by using the Numerov technique [10]. Values of 0.178 and 1.73 were taken for the electron and hole masses, respectively [11].

To take into account the screening of the built-in electric field by photoexcited carriers, the Schroedinger equation was solved self-consistently with the Poison equation [12,13]. Iterative solution of the Schroedinger equation enabled us to calculate the wavefunctions $\Psi_i^{e,h}(x)$ and the spatial distribution of electrons (n^e) and holes (n^h) in the well

$$n^{e,h}(x) = \sum n_i^{e,h} \left| \Psi_i^{e,h}(x) \right|^2 \tag{2.3.1}$$

where $n_i^{e,h}$ is the electron (hole) density in the energy level i, which depends on the Fermi energy and, thus, on the total density of the photogenerated cariers. The resulting charge density distribution was used to calculate the potential profile within the well by employing the Poisson equation,

$$\frac{d^2\phi_i(x)}{dx^2} = \frac{e\left[n_i^e(x) - n_i^h(x)\right]}{\varepsilon\varepsilon_0} \tag{2.3.2}$$

which was discretized and solved by using the tridiagonal matrix technique.

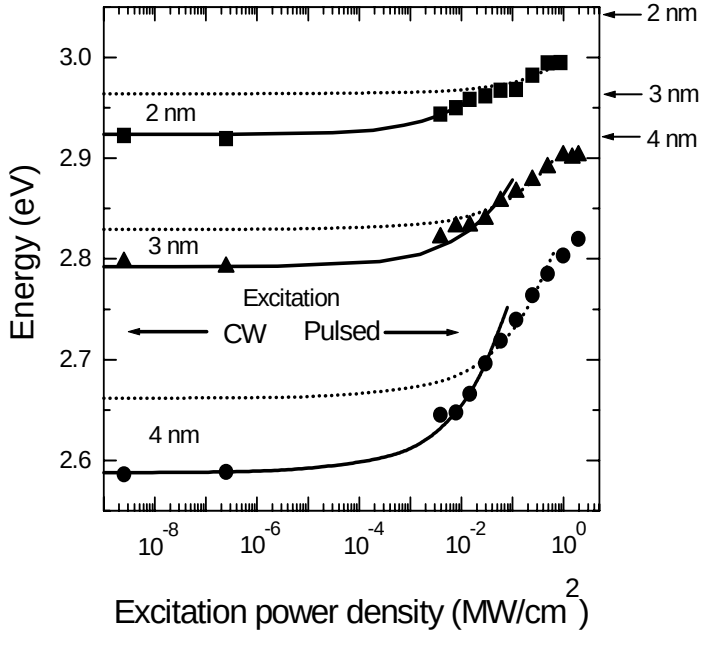

Fig. 2.3.5. Excitation power density dependence of PL peak position in InGaN MQWs with well width of 2 (squares), 3 (triangles), and 4 nm (circles). Lines represent the calculation results best fitted at low (solid line) and high (dotted line) power densities. Arrows indicate the energies of the lowest optical transitions in the quantum wells with corresponding thickness at completely screened built-in electric field (for squared quantum wells).

The calculated carrier density dependence of the lowest energy transition energy was fitted with the experimentally obtained PL peak position dependence on excitation power

density. In the fitting procedure, we supposed that the density of the photoexcited carriers is proportional to a square root of the excitation power density in consistence with the approximately linear excitation power density dependence of the integrated PL intensity, as observed nearly in the whole range of excitation intensities (see Fig. 2.3.3). The calculation results presented in in Fig. 2.3.5 are scaled in units of power density by using this assumption. The upper limit of the calculated dependences is caused by calculation instabilities due to low depth of the quantum well for the holes. The values of the optical transitions in a rectangular quantum well, as a limiting case of complete screening, are pointed in Fig. 2.3.5 by arrows for all three quantum wells with different width, as indicated. As should be expected, the energy difference between the lowest optical transitions in triangle quantum well (no screening effect) and rectangular well (the built-in electrics field is completely screened) increases with increasing well width (see curves (c) and (b) in Fig. 2.3.1b).

2.3.5. Discussion

A reasonable fitting of the calculated blueshift of the lowest optical transition with the experimentally observed blueshift of the PL band peak (see Fig. 2.3.5) was achieved in two limiting cases: either the low-excitation experimental results were best fitted (solid lines in Fig. 2.3.5), either the fitting was based on the high power density region (dotted lines). In the first case the localization of carriers is totally neglected. This is an unrealistic assumption, since carrier (exciton) localization is a well established phenomenon. The second fitting procedure is more realistic. Moreover at low pump intensity, the energy difference between the fitting value (dotted line in Fig. 2.3.5) and the experimentally obtained PL peak position (dots) is a rough estimation of the average localization energy. The results obtained in samples with different well width show that the band redshift due to localization effect does not significantly depend on the well width. Its approximate value of 30-40 meV is close to exciton energy dispersion due to random potential fluctuations, as estimated in $In_{0.2}Ga_{0.8}N$/GaN MQWs (~30 meV) (see Chapter 2.2.). Thus, the redshift of the PL band due to localization becomes less pronounced in comparison with the well tilting as the well width increases. The total blueshift of the PL band with increasing excitation power density seems to be dominated by filling of the localized states at low pump intensities and to becomes governed by screening of the built-in electric field at elevated excitation intensities. The best fit of the calculated carrier density dependence of the lowest optical transition energy with the experimentally measured excitation power density dependence of the PL peak position was achieved at the electric field values of 1.6, 1.35, and 1.5 MV/cm for the well widths of 2, 3, and 4, correspondingly. These are reasonable values for $In_{0.15}Ga_{0.85}N$/GaN interface.

Note pecularities of PL characteristics measured under excitation with photons of different photon energy $h\nu_{exc}$. Provided that the different absorption efficiency is taken into account, the excitation power density dependence of the spectrally integrated PL intensity is analogous for both $h\nu_{exc}$. However, the blueshift of the PL band proceeds faster in case of band-to-band excitation of barrier layers. This is an indication that the screening effect is stronger and, hence, the carrier density is higher when PL of the same intensity is excited via generation of carriers into the barrier layers as compared with selective excitation of the wells.

This behavior might be explained by different conditions for spatial distribution of photoexcited carriers. This distribution is strongly affected by inhomogeneous distribution of In in InGaN quantum wells that results in existence of In-regions with lower potential for photoexcited carriers than the surrounding matrix of InGaN of lower In content [8]. These regions serve for accumulation of the photoexcited carriers to form high-carrier-density regions. As demonstrated by using high-resolution transmission electron microscopy, the In-rich regions tend to form at the well-barrier interface and extend into the barrier, especially when the average In content is increased above 15% [5]. Thus, extension of the In-rich

regions into the barriers improve conditions for the carriers, which are excited in the barrier, to relax directly into these regions. Meanwhile, selective excitation of exclusively well material is less favorable for redistribution of the photoexcited carriers into the In-rich regions provided that the total density of carrier is the same as in the case of barrier excitation.

Note that two PL bands are observed under selective excitation. We suppose that the high-energy band is caused by recombination from the InGaN matrix outside the In-rich regions. Its more pronounced appearance in the spectra measured under selective excitation is consistent with the assumption that the conditions for carrier redistribution into the In-rich regions are harder at selective excitation than that in case of analogous excitation into the barriers.

2.3.6. Conclusions

In summary, comparison of experimentally obtained redshift of PL band with calculated energy of the lowest optical transition in InGaN MQW enables partial separation of contributions of the well tilting due to the quantum-confined Stark effect and the carrier localization that affect carriers accumulated in In-rich regions. As the first step, the increasing carrier generation rate causes filling of the localized states (with typical average localization energy of ~30-40 meV in $In_{0.15}Ga_{0.85}N$). The further increase of excitation intensity causes screening of the built-in electric field and, hence, the further blueshift of the PL band. The screening effect is stronger and, hence, the carrier density is higher when PL of the same intensity is excited via generation of carriers into the barrier layers as compared with selective excitation of the wells. This result is in consistence with existence of In-rich regions, which are formed at the well-barrier interface and extend into the barrier.

References

[1] Y. Narukawa, Y. Kawakami, M. Funato, S. Fujita, S. Fujita, and S. Nakamura, Appl. Phys. Lett. **70**, 981 (1997).
[2] S. Chichibu, K. Wada, and S. Nakamura, Appl. Phys. Lett. **71**, 2346 (1997).
[3] T. Saiki, K. Nishi, M. Ohtsu, Jpn. J. Appl. Phys., Part 1 **37**, 1638 (1998).
[4] N. Duxbury, U. Bangert, P. Dawson, E. J. Thrush, W. Van der Stricht, K. Jacobs, and I. Moerman, Appl. Phys. Lett. **76**, 1600 (2000).
[5] Y. S. Lin, K. J. Ma, C. Hsu, S. W. Feng, Y. C. Cheng, C. C. Liao, C. C. Yang, C. C. Chou, C. M. Lee, and J. I. Chyi, Appl. Phys. Lett. **77**, 2988 (2000).
[6] J. Kim, K. Samiee, J. O. White, J.-M Myoung, and K. Kim, Appl. Phys. Lett. **80,** 989 (2002).
[7] S. Chichibu, T. Sota., K. Wada., S. Nakamura, J. Vac. Sci. Technol. B, **16**, 2204 (1998).
[8] K. Kazlauskas, G. Tamulaitis, A. Žukauskas, M. A. Khan, J. W. Yang, J. Zhang, G. Simin, M. S. Shur, R. Gaska, Appl. Phys. Lett. **83**, 3722 (2003).
[9] C.G.Van der Walle and J.Neugebauer, Appl. Phys. Lett., V. **70**, p.2577, (1997)
[10] P. C. Chow, Amer. J. Phys., **40**, 730 (1972).
[11] Y. C. Yeo, T. C. Chong, and M. F. Li, J. Appl. Phys. **83**, 1429 (1998).
[12] K. S. Lee, D. H. Yoon, S. B. Bae, M. R. Park, G. H. Kim, ETRI Journal, **24**, 270 (2002).
[13] A. M. Cruz Serra and H. Abreu Santos, J. Appl. Phys. **70**, 2734 (1991).

2.4 THERMOACTIVATION SPECTROSCOPY OF CHARGE LOCALIZATION STATES IN INGAN/GAN QUANTUM WELL

By

I.Tale, M. Piesins

Institute of Solid State Physics, University of Latvia,

8 Kengaraga Str. LV-1063 Riga, Latvia.

C. C. Yang

Department of Mechanical Engineering and Graduate Institute of Electro – Optical Engineering,

National Taiwan University, 1, Roosveld Road, Sec. 4, Taipei, Taiwan, R. O.C

Abstract

The deep level transient spectroscopy (DLTS) for investigation of trapping states in GaN muli quantum well structures has been installed and approved. In order to assess the usability of DLTS technique for study the deep trapping levels in multi-quantum well structures both the thermostimulated depolarization (TSD), thermostimulated capacitance relaxation (TSC) and DLTS are studied in p-n homojunction GaN blue diode. The TSD and TSC curves shows that cooling of the GaInN structure down to liquid helium temperatures results in complete trapping both the majority and the minority charge carriers at the shallow dopand levels. Thermal ionization of the dopand states occurs in the temperature region 40 – 60 K. An electron level at E_c-E_t= 0.30 eV is observed. It is shown that DLTS technique extended wit DSD and TSC measurements is suitable for investigation of deep trapping states in MQW structures. Investigation of the photo-filling spectra of trapping states by DLTS it is prospective for selection of the localization of defect states responsible for deep trapping levels in the barrier, wall or interface region of MQW-s.

2.4.1.Introduction

Gallium nitride (GaN) processes some unique features such as large bandgap (3.39 eV), high thermal stability with a large breakdown field of 2MV/cm. These enable GaN to emerge as unique material for multiple applications particularly light emitting diodes, diode lasers, power electronic devices and solar blind ultraviolet detectors [1,2]. However, the performance of devices can be limited by the deep levels present within the GaN bandgap, which act as traps and/or recombination – generation centres. These deep levels cause non-radiative transitions and in some cases are responsible for long wavelength radiative recombination.

The deep levels in GaN, and GaInN, in general, are either related to structural defects like dislocations, native point defects and/or their complex such as nitrogen vacancies [3], or impurity-related defects.

Doping of GaN may introduce deep levels, in addition to shallow donor or acceptor levels. For example, it has been stated that Mg doping introduces a deep level at $E_c - E_t \sim$ 0.58-0.62 eV. [4]. For Si-doped GaN trap levels at 0.28 and 0.45 eV are attributed to the Si-related defects [5].

At present experimental data concerning deep levels in Ga - related nitride materials condign on self in investigation of pure or doped GaN and GaN homostructures. Studies of trapping levels in GaN heterostructures including quantum well (QW) structures up to now have not been reported. Formation of deep levels in InGaN alloys may considerably affect the electrical characteristics of material as well as charge carrier generation – recombination kinetics.

It can been expected that by increase of the In – content in alloy a selective formation of localized states will occur. It is well known that the poor thermal stability of InN and low In vapor pressure over the metal phase result in the formation of In clusters, especially at temperatures $T > 500$ ^{o}C [7]. It is found that deviations in presently available experimental data on the bandgap of InN from 0.7 to 2 eV[8- 11] are linked to the precipitation of indium in the metallic phase that leads to additional optical losses due to light scattering and absorption by dispersed small particles [12].

Additional reason for formation of localized electron states is disorder in the interface region barrier-wall in the MQW-s of GaN/InGaN. Deep levels due to self – organized quantum dots (QD) may significantly affect the light generation processes. Particularly it is stated that self-organized InAs quantum dots (QD) embedded in GaAs act as both the electron and the hole trapping centres [6]. Thus, QD can act as radiative recombination centres. However, investigations of hole and electron escape from a single layer QD in GaAs matrix by time-resolved capacitance spectroscopy show fundamentally different behavior. For electrons, besides conventional tunnel emission a thermally activated tunneling processes involving excited QD states dominates for high temperatures. For holes only thermal activation from the ground state directly to the GaAs valence band contributes. It is stated that the hole localization time at given temperature in the QD is significantly larger than the one of electrons. In GaInN/GaN both the carrier trapping and the strain-induced piezoelectric field, which generates the quantum confined Stark effect, has been involved for interpreting observed optical phenomena in samples with increasing silicon-doping concentration, such as the photoluminescence peak shift and decay time decrease followed by intensity increase [13-15]. The temperature dependence of photoluminescence has been interpreted assuming capture and thermoactivated delocalization of excitons from QD [13].

It can be expected that like other structure defects and impurities the QD will act as deep capture centers for charge carriers. By injection or photo-generation of free electrons and holes subsequent capture of charge carriers in QD can be important formation mechanism of excitons. As result, the composition and the concentration of In clusters significantly depends on the In concentration in WQ as well as the sample thermal annealing conditions.

The objective of the present work is application of the complex of methods of thermoactivation spectroscopy of defects for detailed characterization of localized s in InGaN/GaN quantum well structures. Different methods are utilized to investigate the relative concentration and the thermal activation energy of charge carrier release of various defects: thermostimulated capacitance decay (TSCD), thermostimulated depolarization currents (TSDC) and deep level transient spectroscopy (TLDS).

2.4.2.Experimental

The TSCD, TSDC trap spectroscopy have been performed using closed cycle cryostat in the temperature region, starting from ~10 ^{o}K to about 350 ^{o}K with the linear heating rate being either 0.05 or 0.2 ^{o}Ks^{-1}. Polarization of the sample before TSDC measurements have been carried out in an external field (-30 V) either in the course of slow cooling from ~300 ^{o}K, or by the irradiation with photo-active light at 10^{o}K.

The TLDS trap spectroscopy has been performed using conventional equipment. The closed cycle cryostat was equipped with two screened high impedance, non – vibrating wires attached to the sample holder. The sample mounted was on the sample holder, sample electrical contacts was connected with signal input –output wires using Cu or Ag wires Φ= 0.05 mm. For capacitance and conductance kinetics measurements the Model Boonton 7200 Capacitance meter was utilized. The type Agilent 33220A pulse generator was used as a sample polarization source. The measurement was carried out Five times with different rate windows from 1 ms to q16 ms. The bias used U_b = -1V; The pulse parameters: U_p = 1V; Δt=1 ms. The Commercial blue light diode was used for investigations.

2.4.3. Results

For the general characterization of the donor/acceptor doping governed diode conductivity parameters the temperature dependence of the conductivity and capacity was investigated. By cooling down up to about 80 K both the conductivity and the capacity decrease only slightly.

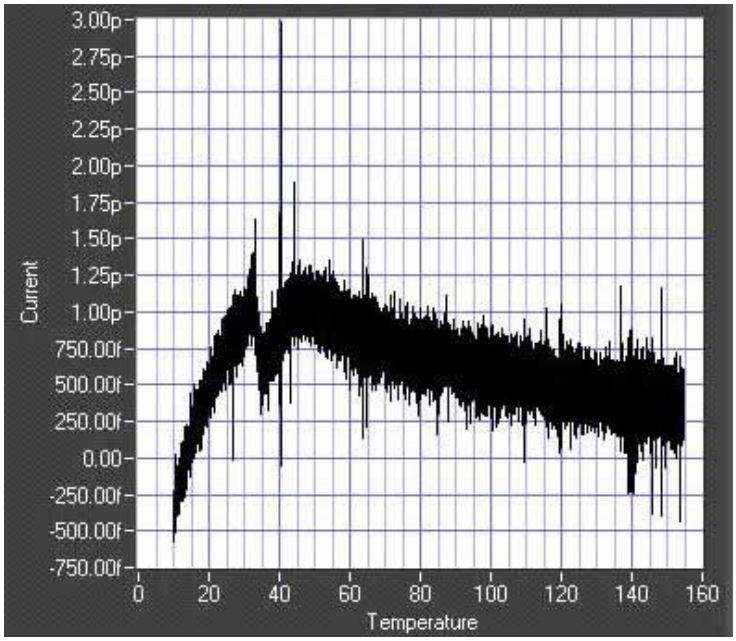

Figure 2.4.1. The depolarization current of the diode, polarized by cooling down of the sample to 10 K by applied bias -20 C, and heated with constant rate).1 K/s

Further cooling results in decrease of conductivity from the value of about 80 μS to the very low value. The later is close to the sensitivity limit of the capacitance meter. Simultaneously capacitance decreases from 64pF, to 0.2 pF. Results indicate that at low temperatures the donors are going occupied by electrons. The capacity at high temperatures being caused by p-n transition capacity at low temperatures reflects the sample capacity wit GaInN as dielectric media.

For study of the TSCD and TSDC the sample has been cooled down in external field (U_b=-25V) to T=10 K . Fig.2.4.1 represents the temperature dependence of depolarization current recorded by heating rate 0.1 K/s. Depolarization curve shows presence of two stages of depolarization kinetics. The observed kinetics indicates that two kinds of donor which differ in activation energy are present in MQW structure. It can be proposed the low temperature peak origins due to escape of electrons from donor states in the well region whereas the high temperature peak, characterized by more high activation energy correspond escape of electrons in GaN.

Results of the DLTS measurements provided at different temperatures are represented in Figure 2.4.2. By applying a voltage pulse the measured capacitance increases and remains

constant until the end of the pulse. At the end of the pulse the capacitance falls below the original level. After that time the capacitance increases exponentially.

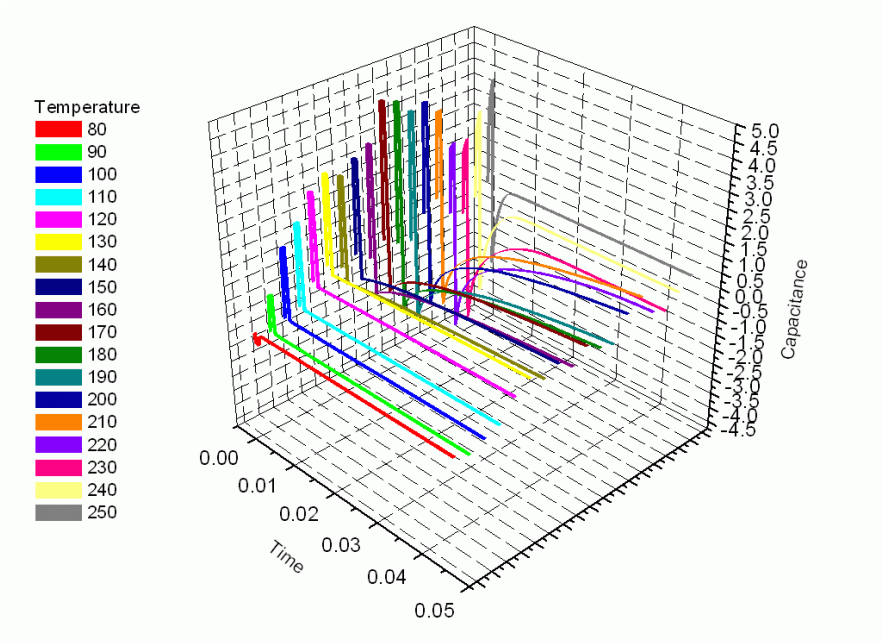

Figure 2.4.2. The capacitance transient kinetics obtained at different temperatures.

The Figure 2.4.3 shows the DLTS spectrum for the MQW structure obtained at different rate windows. At different rate windows the shape of the DLTS spectrum remains unchanged. This result indicates that the single deep trapping level represents the main localized state in the MQW structure.

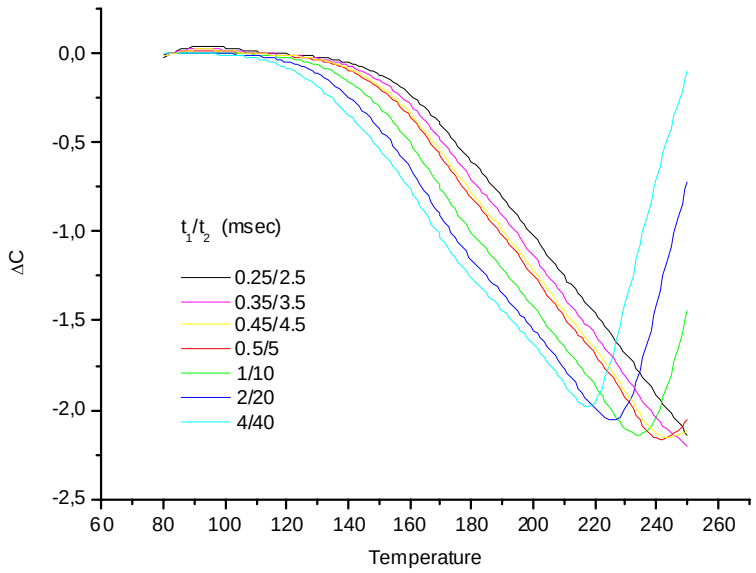

Figure 2.4.3. DLTS spectra of the GaN MQW structure obtained at different rate windows.

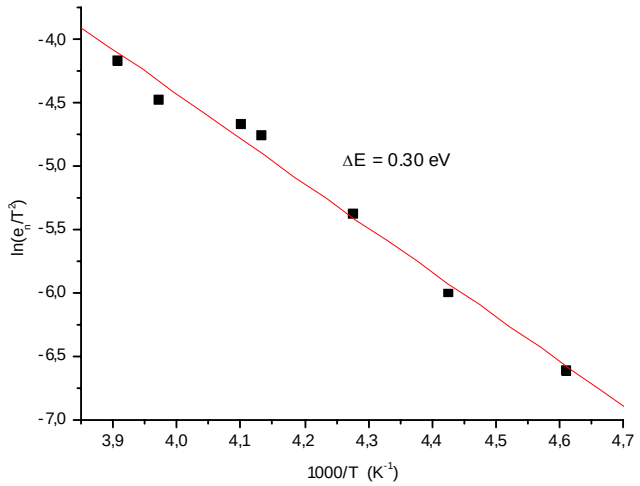

Figure 2.4.4. Arrhenius plot of deep defect levet in the GaN MQW structure. The activation energy of the traps : 0.30 eV

2.4.4.Conclusion

In order to assess the usability of DLTS technique for study the deep trapping levels in multi-quantum well structures both the thermostimulated depolarization (TSD), thermostimulated capacitance relaxation (TSC) and DLTS are studied in p-n homo-junction GaN blue diode. The TSD and TSC curves shows that cooling of the GaInN structure down to liquid helium temperatures results in complete trapping both the majority and the minority charge carriers at the shallow dopand levels. Thermal ionization of the dopand states occurs in the temperature region 40 – 60 K.

Two kinds of donor levels governing the conductivity at high temperatures are observed in the MQW structures which have close activation energies. It is proposed that they characterize the dopand energy in walls and barriers respectively.

According to the DLTS spectra the single deep electron level at E_c-E_t= 0.30 eV is observed. It is shown that DLTS technique extended with TSD and TSC measurements is suitable for investigation of deep trapping states in MQW structures. Investigation of the photo-filling spectra of trapping states by DLTS it is prospective for selection of the localization of defect states responsible for deep trapping levels in the barrier, wall or interface region of MQW-s.

References

1. Zhang X, Chua S J, Liu W & Li P, Phys. Stat. Solidi, **216**, No.307, 307 (1999)

2. S. Nakamura, M. Senoch, S. Nagahama, N. Iwasa, T. Yamada, T. Matsushita, H. Kiyoka, and Y. Sugimoto, Jpn. J. appl. Phys., Part 2 **35**, L74, 1996.

3. Z-Q. Fang, J.W. Hemsky, D.C.Look, and M.P. Mack, Appl. Phys. Lett. **72**, 448 (1998)

4. A. Hierro, S.A. Ringel, M. Hansen, J.S. Speck, U.K. Mishra and S.P. DenBaars, Appl. Phys Lett. **77**, 1499 (2000).

5. C.B. Soh, D.Z. Chi, H.F.Lim and S.J. Chua, Mat. Res. Soc. Symp. Proc. **719,** F13.5 (2002).

6. C. M. A. Kapetyn, M. Lion, R. Heitz, D. Bimberg, P.N. Brunkov, B. V. Volovik, S. G. Konnikov, A. R. Kovsh, and V. M. Ustinov, Appl. Phys. Lett. **76**, 1573 (2000).

7. S. V. Ivanov and V. N. Jmerik, in *Vacuum Science and Technology: Nitrides as Seen by the Technology,* ed. By T. Paskova and B. Monemar (Research Signpost, Kerala, 2002), p. 369.

8. L. Tansley and C.P. Foley, J. Appl. Phys. **59**, 3941 (1986)

9. T. Inushima, V. V. Mamutin, V. a. Vekshin, S. V. Ivanov, T. Sakon, M. Motokawa, and S. Okoya, J. Cryst. Growth **227/228**, 481 (2001)

10. V. U. Davydov, A. A. Klochikhin, R. P. Seisyan, V. V. Emtsev, S. V. Ivanov, F. Bechstedt, J. Furthmueler, H. Harima, A. V. Mudryi, J. Aderhold, O. Semchinova, and J. Graul, Phus. Status Solidi B **229**, R1 (2002).

11. J. Wu, W. Walukiewicz, K. M. Yu, J. W. Ager III, E. e. Haller, H. Lu, W. J. Schaff, Y. Saito, and Y. Nanishi, Appl. Phys. Lett. **80**, 3967 (2002).

12. T.V. Shubina, S. V. Ivanov, V. N. Jmerik, D. D. Solnyshkov, V. A. Vekshin, P. S. Kop'ev, A. Vasson, J. Leymarie, A. Kavokin, H. Amano, K. Shimono, A. Kasic, and B. Monemar., Phys. Rev. Lett. **92**, 117407-1 (2004).

13. Yung-Chen Cheng, Cheng-Hua Tseng et al. Appl. Phys. Lett., June 2002

14. P. Ramvall, Y. Aoyagi, A. Kuramata, P. Hacke, K. Domen, and K. Horino, Appl. Phys. Lett. **76**, 2994 (2000).

15. E. Oh, C. Sone, O. Nam, H. Park, and Y. Park, Appl. Phys. Lett. **76**, 3242 (2000).

2.5. NANOSTRUCTURES AND CARRIER LOCALIZATION BEHAVIORS OF GREEN-LUMINESCENCE InGaN/GaN QUANTUM-WELL STRUCTURES OF VARIOUS SILICON-DOPING CONDITIONS

By
Yung-Chen Cheng, En-Chiang Lin, Cheng-Ming Wu, C. C. Yang, and Jer-Ren Yang
Graduate Institute of Electro-Optical Engineering, Graduate Institute of Electronics Engineering, Department of Electrical Engineering, and Department of Material Science and Engineering,
National Taiwan University, Taipei, Taiwan, R.O.C.
Andreas Rosenauer
Laboratorium für Elektronenmikroskopie, Universität Karlsruhe, Germany
Kung-Jen Ma
Department of Mechanical Engineering, Chung Hua University, Hsinchu, Taiwan, R.O.C.
Shih-Chen Shi and L. C. Chen
Center for Condensed Matter Sciences, National Taiwan University, Taipei, Taiwan, R.O.C.
Chang-Chi Pan and Jen-Inn Chyi
Department of Electrical Engineering, National Central University, Chung-Li, Taiwan, R.O.C.

Abstract

The results of photoluminescence (PL), detection-energy-dependent photoluminescence excitation (DEDPLE), excitation-energy-dependent photoluminescence (EEDPL), and strain state analysis (SSA) of three InGaN/GaN quantum-well (QW) samples with silicon doping in the well, barrier and an undoped structure are compared. The SSA images show strongly clustering nanostructures in the barrier-doped sample and relatively weaker composition fluctuations in the undoped and well-doped samples. Differences in silicon doping between the samples give rise to the differences in DEDPLE and EEDPL spectra, as a result of the differences in carrier localization. Also, the PL results provide us clues for speculating that the S-shape PL peak position behavior is dominated by the quantum-confined Stark effect in an undoped InGaN/GaN QW structure.

2.5.1. Introduction

Silicon doping in InGaN/GaN quantum wells (QWs) has been widely used in fabricating high performance light emitting devices. Silicon doping has been reported to affect many properties of InGaN/GaN QWs, including the growth mode change [1], the microstructure (through the formation of quantum dots (QDs)) [2], the interface abruptness [3], the photoluminescence (PL) intensity [4-6], the uniformity of the potential in the well [1,7], the strain relaxation [8], and the screening of piezoelectric field [9-11]. However, most previous studies of silicon doping effects focused on the samples emitting violet-blue photons. Silicon-doped InGaN/GaN QWs of higher nominal indium contents, leading to green light emission, were rarely investigated. Also, the nanostructures and their implications in radiative mechanisms of such silicon-doped samples, emitting either violet-blue or green light, have not been well studied yet. Usually, it is difficult to grow uniform InGaN alloy, particularly with high indium contents. This is so due to the solid phase immiscibility and phase separation between GaN and InN [12], which originate from their large lattice constant mismatch.

In this letter, we report the comparisons of nanostructure and related optical characteristics between green-emitting InGaN/GaN QW samples of the same geometry and composition, but different silicon doping conditions. Three samples of no doping, well doping, and barrier doping were prepared for comparisons. Detection-energy-dependent

photoluminescence excitation (DEDPLE) and excitation-energy-dependent photoluminescence (EEDPL) measurements show different variation trends of absorption spectrum and PL spectral peak position, respectively. Such trends can be well interpreted with the observations of strain state analysis (SSA), based on a high-resolution transmission electron microscopy technique [13].

2.5.2. Experimental

The three InGaN/GaN QW samples of different doping conditions were prepared with MOCVD growth on sapphire (0001) substrate. They all consisted of five QW periods, with 2.5 nm in well width and 7.5 nm in barrier width, on top of an un-doped GaN buffer layer of 1.52 μm in thickness. The growth temperatures were 1100 and 800 ^{o}C for the GaN barriers and InGaN wells, respectively. The doping concentration of silicon was 5 x 10^{18} cm^{-3}, either in barriers or wells. The samples with un-doped, well-doped and barrier-doped conditions were denoted with HU, HW, and HB, respectively. The nominal indium contents of the three samples are the same at 20 %.

2.5.3. Results and discussion

Figs. 2.5.1(a) and (b) show the temperature-dependent variations of PL spectral peak and normalized integrated PL intensity, respectively, of the three samples. From part (a), one can see the blue shift of sample HB when compared with samples HU and HW. Only sample HU generates a clear S-shape variation [14].

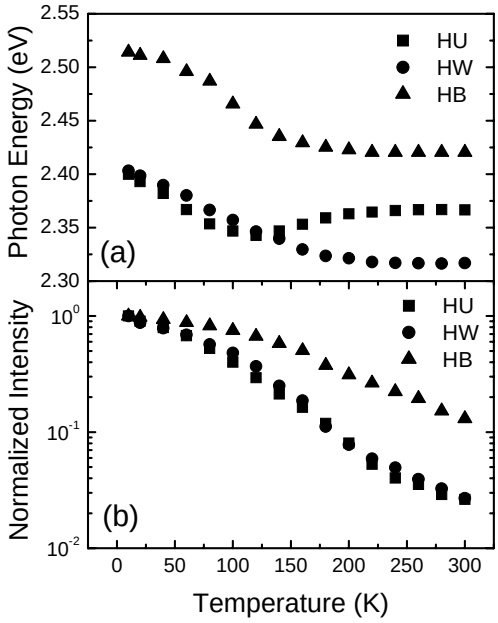

Fig. 2.5.1 (a) Temperature-dependent PL spectral peak positions, and (b) integrated PL intensities of the three samples

As shown in Fig. 2.5.1(b), the radiative efficiency of sample HB is higher than those of the other two samples. Such results are quite similar to what we have reported previously with the samples emitting violet photons [2]. Barrier-doped samples always result in higher optical quality. Fig. 2.5.2 shows the PL and DEDPLE spectra of the three samples at 10 K.

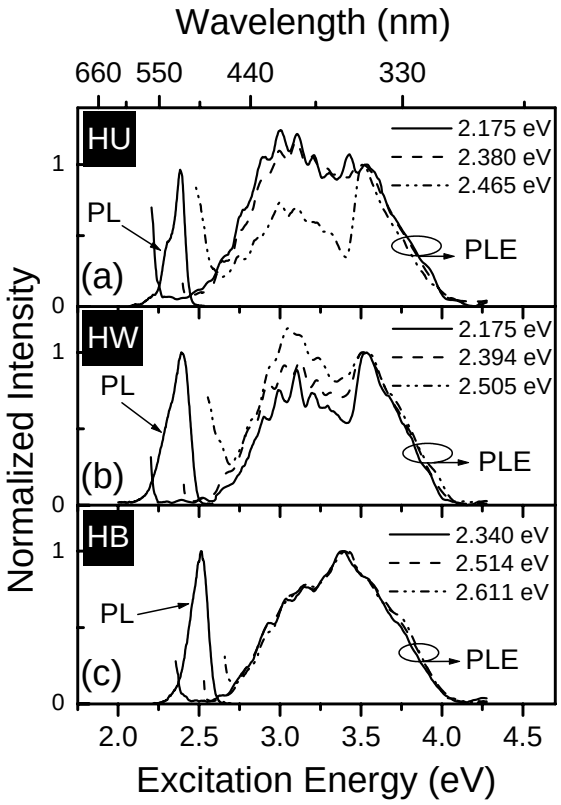

Fig. 2.5.2 PL and DEDPLE spectra of the three samples. The eV values shown are the detection photon energies.

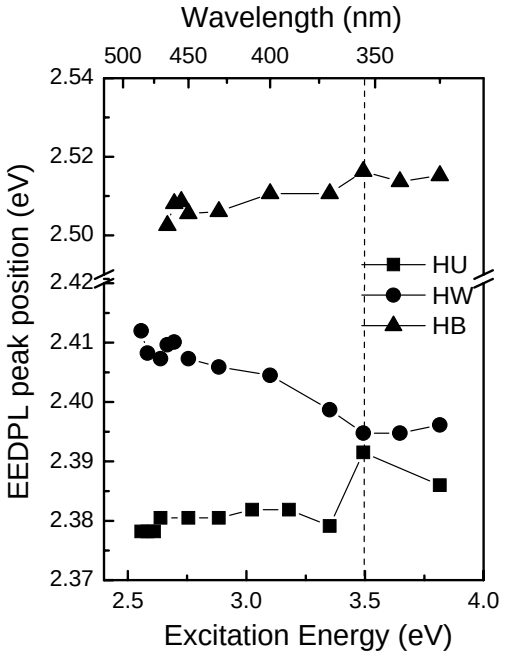

Fig. 2.5.3. EEDPL spectral peak positions as functions of excitation photon energy of the three samples.

The DEDPLE spectra were normalized to the level at 3.5 eV (GaN absorption peak). One can see that in sample HU, the luminescence intensity level of the InGaN absorption band decreases with increasing detection photon energy. However, the opposite variation trend is observed in sample HW. Meanwhile, almost the same absorption spectra, when the detection photon energy is varied, are measured in sample HB. Such major differences imply the significant variations in sample nanostructure upon silicon doping of different conditions. Fig. 2.5.3 shows the EEDPL spectral peak positions as functions of excitation photon energy for the three samples. In sample HU, the EEDPL spectral peak maintains almost constant

when carriers are excited in InGaN. That of sample HW increases with decreasing excitation energy. However, the opposite trend is observed in sample HB.

Figs. 2.5.4-6 show typical SSA images of samples HU, HW, and HB, respectively. In these SSA images, line scans were conducted along the shown white lines. Here, the line scan values 1 and 1.1, respectively, represent indium compositions of 0 and 60 % (estimated based on the assumption of a specimen thickness larger than 30 nm). Different colors stand for various ranges of indium composition, as shown in the legends.

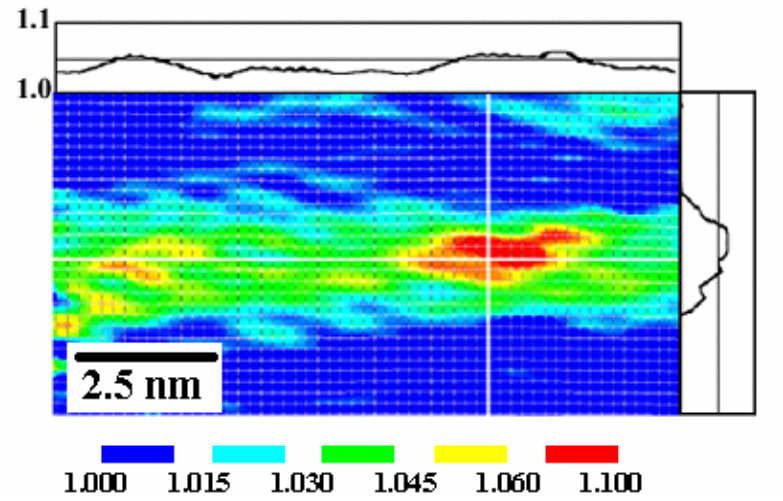

Fig. 2.5.4. A typical strain-state analysis (SSA) image of the undoped InGaN/GaN quantum well sample HU. The color legend indicates the estimated indium mole fractions (1.0 = 0 %, 1.1 = 60 %).

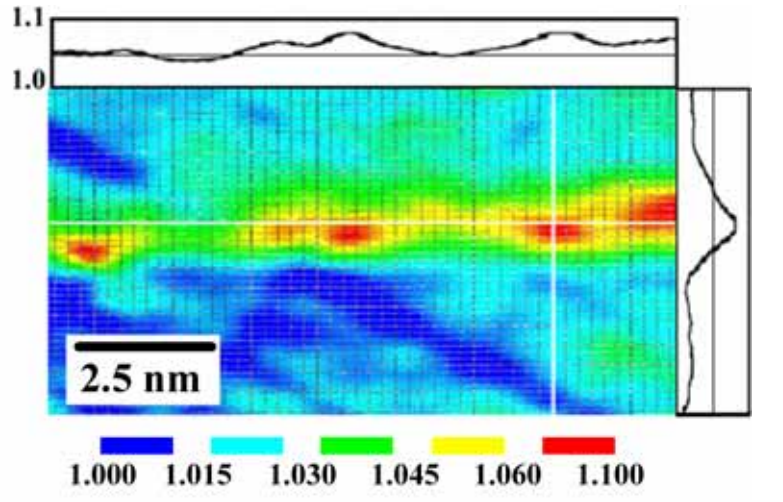

Fig. 2.5.5. A typical strain-state analysis (SSA) image of the well-doped InGaN/GaN quantum well sample HW. The color legend is the same as that in Fig. 2.5.4.

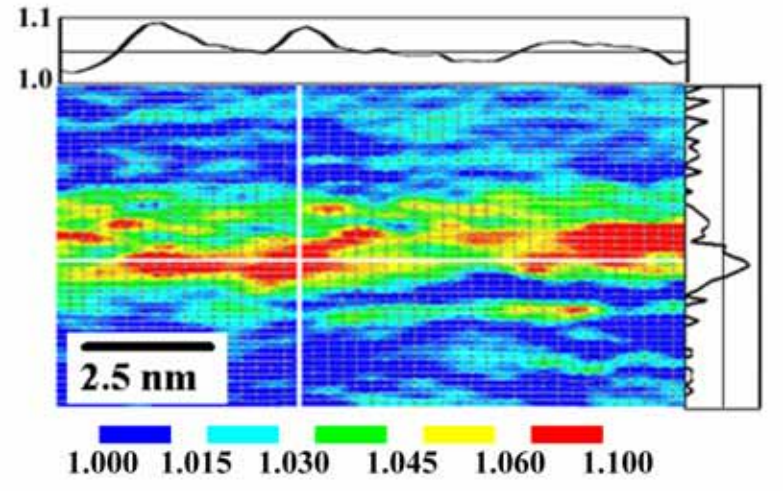

Fig. 2.5.6 A typical strain-state analysis (SSA) image of the barrier-doped InGaN/GaN quantum well sample HB. The color legend is the same as that in Fig. 2.5.4.

As shown in Fig. 2.5.4 for sample HU, although the QW interface is blurred, indium is basically confined within the well. Here, within the well a few spots of indium aggregation can be observed. From the line-scan results, one can observe quite a weak fluctuation in indium composition either along the well layer or in the growth direction. The fluctuation contrast (the difference between the maximum and minimum in the scan range) is around 0.03 along the QW layer.

Then, in Fig. 2.5.5 for sample HW, the QW is not as well shaped as sample HU. The indium composition fluctuations in both directions are relatively stronger in comparing with sample HU. In particular, more indium-aggregated clusters can be observed within the well layer. The fluctuation contrast is now around 0.045 along the QW layer. As shown in Fig. 2.5.6, the SSA image of sample HB shows quite a different nanostructure from the other two samples. Here, the QW layer becomes unclear. Instead, a distribution of clusters of different sizes and shapes exists. The indium composition fluctuation (the contrast is now around 0.075 along the QW layer) is much stronger than those of the other two samples, implying stronger carrier localization for effective recombination.

In Fig. 2.5.2(a), the DEDPLE signal intensity decreases with increasing detection photon energy in sample HU. This trend can be attributed to the relatively weaker potential fluctuation in this sample. With such an energy level distribution, photo-generated carriers in higher energy levels can easily transport to the absolute potential minimum for recombination within a certain region. Hence, when the detection photon energy is low, most carriers can contribute to photon emission. When the detection photon energy is higher, fewer carriers can actually recombine at this relatively higher energy level and hence the DEDPLE signal becomes weaker. In this situation, PL spectral peak is always located at the absolute potential minimum and is independent of the excitation level, as shown in Fig. 2.5.3. On the other hand, in sample HW the potential fluctuation becomes relatively stronger. In particular, more clusters are formed in the designated QW layers (see Fig. 2.5.5). In this situation, it requires certain amount of energy and hence is more difficult for carriers to transport from a local minimum to another of a deeper level. Therefore, the majority of photo-generated carriers can be trapped by local minima of relatively higher energy. When the detection photon energy is high, stronger DEDPLE signals are recorded, as shown in Fig. 2.5.2(b). In this case, as the excitation energy becomes lower in the EEDPL measurement, more carriers can actually be trapped in local potential minima of relatively higher levels such that the PL spectral peak energy increases with decreasing excitation energy, as shown in Fig. 2.5.3. Then, in sample HB, because of the strongly clustering structure with an island-by-island configuration (see Fig. 2.5.6), when carriers are generated at high InGaN energy levels, they can transport directly into individual potential minima without a cascading relaxation process. In this situation, carrier distributions after relaxation among shallow and deep potential minima can be quite even such that the DEDPLE signal intensity is almost independent of the detection photon energy. Also, as the excitation photon energy decreases, the local potential minima of relatively lower levels can collect more carriers and hence the EEDPL peak position decreases.

Carrier localization and quantum-confined Stark effect (QCSE) have been the two major mechanisms for explaining the S-shape behavior of temperature dependent PL spectral peak position. However, it is still unclear which one dominates under a certain condition. With the results above, one can speculate that upon silicon doping in wells or barriers, the QCSE is reduced, due to strain relaxation and/or carrier screening, and the S-shape behavior disappears in samples HW and HB (see Fig. 2.5.1). This argument actually implies that the usually observed S-shape behavior can be dominated by the QCSE. On the other hand, carrier localization can be the key to the blue shift and radiative efficiency improvement, particularly in the barrier-doped sample. The similar nanostructures of samples HU and HW explain well their close PL spectral peak positions, particularly below 150 K, and their close integrated PL

intensity curves. The stronger carrier localization in sample HB does result in higher radiative efficiency. This result may imply that carrier localization is more effective in blue-shifting luminescence and improving radiative efficiency of a sample, when compared with the relaxation of QCSE.

2.5.3. Conclusions

In summary, we have compared the results of PL, DEDPLE, EEDPL, and SSA of three InGaN/GaN QW samples with un-doped, well-doped, and barrier-doped structures. The SSA images showed strongly clustering nanostructures in the barrier-doped sample and relatively weaker composition fluctuations in the undoped and well-doped samples. Such variations in nanostructure resulted in different carrier transport processes that well explained the DEDPLE and EEDPL observations. Also, the PL results provided us clues for speculating that the S-shape PL peak position behavior is dominated by the QCSE in an undoped InGaN/GaN QW structure. However, carrier localization is more effective in blue-shifting luminescence and improving radiative efficiency of a sample, when compared with the relaxation of QCSE.

References

1. K. Uchida, T. Tang, S. Goto, T. Mishima, A. Niwa, J. Gotoh, Appl. Phys. Lett. **74**, 1153 (1999).
2. Y. C. Cheng, Cheng-Hua Tseng, Chen Hsu, Kung-Jen Ma, Shih-Wei Feng, En-Chiang Lin, C. C. Yang, and Jen-Inn Chyi, J. Electron. Mater. **32**, 375 (2003).
3. Y. H. Cho, F. Fedler, R. J. Hauenstein, G. H. Park, J. J. Song, S. Keller, U. K. Mishra and S. P. DenBaars, J. Appl. Phys. **85**, 3006 (1999).
4. M. S. Minsky, S. Chichibu, S. B. Fleischer, A. C. Abare, J. E. Bowers, E. L. Hu, S. Keller, U. K. Mishra and S. P. DenBaar, Jpn. J. Appl. Phys. **37**, L1362 (1998).
5. T. Deguchi, A. Shikanai, K. Torii, T. Sota, S. Chichibu and S. Nakamura, Appl. Phys. Lett. **72**, 3329 (1998).
6. T. Wang, H. Saeki, J. Bai, T. Shirahama, M. Lachab, S. Sakai and P. Eliseev, Appl. Phys. Lett. **76**, 1737 (2000).
7. J. Dalfors, J. P. Bergman, P. O. Holtz, B. E. Sernelius, B. Monemar, H. Amano and I. Akasaki, Appl. Phys. Lett. **74**, 3299 (1999).
8. S. Ruvimov, Z. Liliental-Weber, T. Suski, J. W. Ager III, J. Washburn, J. Krueger, C. Kisielowski, E. R. Weber, H. Amano and I. Akasaki, Appl. Phys. Lett. **69**, 990 (1996).
9. E. Oh, C. Sone, O. Nam, H. Park and Y. Park, Appl. Phys. Lett. **76**, 3242 (2000).
10. M. Y. Ryu, P. W. Yu, E. J. Shin, J. I. Lee, S. K. Yu, E. Oh, O. H. Nam, C. S. Sone and Y. J. Park, J. Appl. Phys. **89**, 634 (2001).
11. C. K. Choi, Y. H. Kwon, B. D. Little, G. H. Gainer, J. J. Song, Y. C. Chang, S. Keller, U. K. Mishra and S. P. DenBaars, Phys. Rev. B, **64**, 245339-1 (2001).
12. I. Ho, G. B. Stringfellow, Appl. Phys. Lett. **69**, 2701 (1996).
13. D. Gerthsen, B. Neubauer, A. Rosenauer, T. Stephan, H. Kalt, O. Schon and M. Heuken, Appl. Phys. Lett. **69**, 2701 (1996).
14. Y. H. Cho, G. H. Gainer, A. J. Fischer, J. J. Song, S, Keller, U. K. Mishra, and S. P. DenBaars, Appl. Phys. Lett. **73**, 1370 (1998).

2.6 IMPROVEMENTS OF InGaN/GaN QUANTUM WELL INTERFACES AND RADIATIVE EFFICIENCY WITH InN INTERFACIAL LAYERS

By
Yung-Chen Cheng, Cheng-Ming Wu, Meng-Kuo Chen, C. C. Yang, Zhe-Chuan Feng
Graduate Institute of Electro-Optical Engineering, Graduate Institute of Electronics Engineering, and Department of Electrical Engineering, National Taiwan University, Taipei, Taiwan, R.O.C.
Gang Alan Li
ShenZhen FangDa GuoKe Optronics Technical Co. Ltd. ShenZhen City, China
Jer-Ren Yang
Department of Material Science and Engineering, National Taiwan University, Taipei, Taiwan, R.O.C.
Andreas Rosenauer
Laboratorium für Elektronenmikroskopie, Universität Karlsruhe, 76128 Karlsruhe, Germany
Kung-Jen Ma
Department of Mechanical Engineering, Chung Hua University, Hsinchu, Taiwan, R.O.C.

Abstract:
The optical properties and nanostructures of two InGaN/GaN quantum well (QW) samples of slightly different structures are compared. In one of the samples, InN interfacial layers of a couple mono-layers are added to the structure between wells and barriers for improving the QW interface quality. Compared with the standard barrier-doped QW sample, the addition of the InN interfacial layers does improve the QW interface quality and hence photon emission efficiency. The strain state analysis images show the high contrast between the clear QW interface in the sample with InN layers and the diffusive QW boundaries in the reference sample. The detection-energy-dependent photoluminescence excitation data reveal the consistent results.

2.6.1 Introduction

Due to the large lattice mismatch between InN and GaN, it is usually difficult to grow high-quality InGaN/GaN quantum wells (QWs) [1-4]. In particular, the diffusive interface between a well and a barrier usually leads to poor quantum confinement and hence lower photon emission efficiency. Also, with the diffusive QW structures, it becomes difficult to predict and hence design the emission wavelength for practical light-emitting devices. Furthermore, the low-quality interface may result in defect states and hence deteriorate the performance of such a light-emitting device [5,6]. The diffusive QW interfaces can be attributed to the migrations of indium and gallium atoms through spinodal decomposition and other strain-induced effects. Although such processes can result in the formation of quantum dot-like clusters for localizing carriers and hence effective recombination [7-9], defects like dislocations may exist at the boundaries of the clusters [10], leading to the degradation of the photon emission efficiency. Therefore, the improvement of QW quality, particularly the interfacial quality, is very important for the development of the related light-emitting devices.

In this letter, we compare the photoluminescence (PL) and electro-luminescence (EL) properties of two InGaN/GaN QW samples with different well/barrier interface structures. InN thin layers of about 1 nm in thickness are inserted between a well and the neighboring barriers for improving the interfacial quality. From optical characterization and nanostructure

analysis (strain state analysis -- SSA), it is found that with the InN interfacial layers, photon emission efficiency is improved, when compared with a standard InGaN/GaN QW sample of barrier doping.

2.6.2 Experimental

The two InGaN/GaN QW samples were grown on c-plane sapphire with MOCVD. After a 4-μm Si-doped GaN (4 x 10^{18} cm^{-3} in doping concentration) layer, eight periods of QW were grown with 2.5 nm in well width and 13.5 nm in barrier width. The barriers were Si-doped with 5 x 10^{17} cm^{-3} in doping concentration. The nominal indium content of the InGaN wells was estimated to be 20 %. On top of the QW layers, a 150 nm p-GaN layer (3 x 10^{17} cm^{-3} in carrier concentration) was grown for preparing Ohmic contact. The sample described above is designated as sample B. In sample A, a Si-doped InN thin layer of about 1 nm in thickness was inserted into the sample between a well and its neighboring barrier on either side. Ohmic contacts were prepared for EL measurements. The growth temperatures for all layers were the same at 735 ^{o}C with very low growth rates and high V/III ratios. In the PL measurements, the excitation power was minimized to avoid the carrier effects. The injection currents in the EL measurements for samples A and B were 1.1 and 1.5 mA, respectively. The electric current levels were designated right above the threshold values for effective output detection. The comparison of injection current shows that sample A is superior to sample B in EL performance.

2.6.3 Results and discussion

Fig. 2.6.1 shows the PL and EL spectra of the two samples at several temperatures.

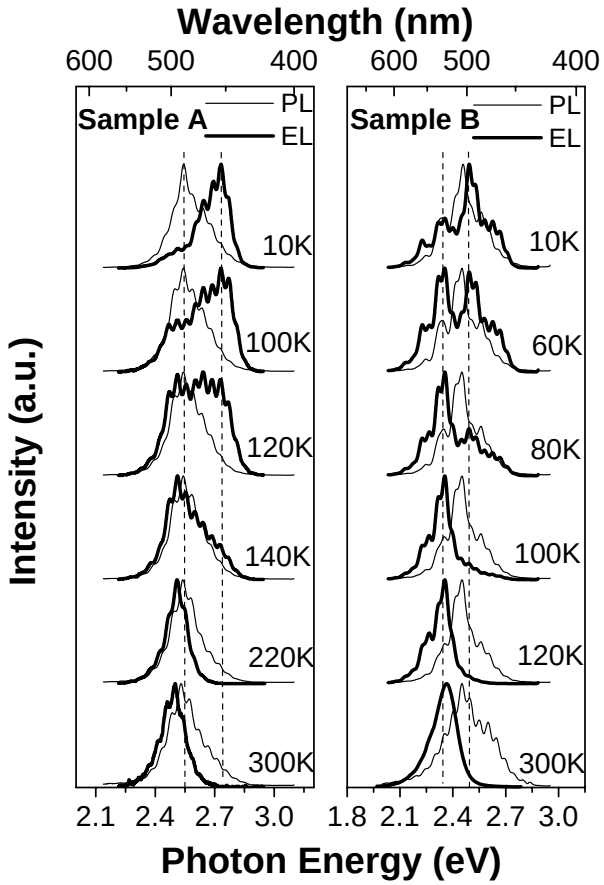

Fig. 2.6.1 PL (thin lines) and EL (thick lines) spectra of the two samples at various temperatures. Two peaks can be observed in some cases of low temperatures.

Although Fabry-Perot oscillations are quite strong in these spectra, the single peak positions of PL spectra can be easily identified. In the EL spectra, two peaks can be observed,

particularly at low temperatures. In either sample, the major part of EL intensity shifts from the higher energy peak to the lower one as temperature increases [11]. In the middle range of temperature, both peaks exist. The red-shift trend with increasing temperature, shown in Fig. 2.6.1, is opposite to the previously reported blue-shift behavior [12]. Fig. 2.6.2 summarizes the PL and EL spectral peak positions of the two samples.

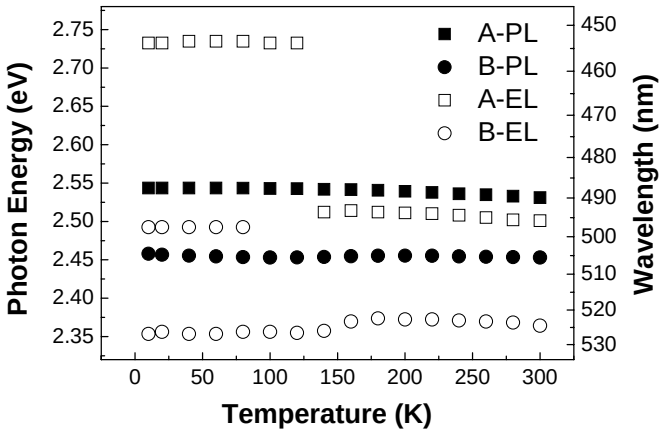

Fig. 2.6.2 PL and EL spectral peak positions of the two samples as functions of temperature. The two peaks are shown whenever they are clear for calibration.

In sample B, the higher-energy peak exists up to 80 K. In sample A, the higher-energy peak exists up to 120 K and the lower-energy peak cannot be identified below this temperature. In both samples, PL spectral peaks lie between the two EL peaks in the whole temperature range. The higher-energy peaks in the EL spectra can be attributed to the carrier activities in the QW energy states (or called free-carrier states). The lower-energy peaks correspond to those around the potential minima of clusters (or called localized states) within QWs [13,14]. The localized states are also responsible for the PL emission. The localized-state-related EL is red-shifted from PL in both samples. This trend can be attributed to the application of forward bias voltage in current injection for EL measurements. With the forward bias, the originally existing potential slope (due to the piezoelectric field) is further tilted, leading to a stronger quantum-confined Stark effect (QCSE) and hence the red shifts. The QCSE can be partially compensated by the carrier screening effect with carrier injection, which can reduce the potential tilt. From the results in Fig. 2.6.2, one can speculate that the effective potential tilt increment due to current injection in sample A is smaller. Hence, the differences between the localized-state-related EL and PL spectra of sample A are smaller. In other words, it is easier to design light emission wavelength of a practical device based on the PL measurement with an epi-structure like sample A.

Fig. 2.6.3 shows the normalized integrated intensities of PL and EL as functions of temperature in the two samples. The decay slope of such a curve represents the radiative efficiency of a sample. Here, one can see that in either PL or EL measurement, the radiative efficiency of sample A is significantly higher than that of sample B. The addition of the InN interfacial layer can help in improving the photon emission efficiency.

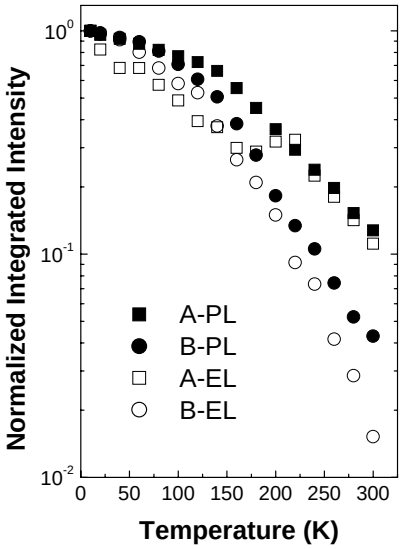

Fig. 2.6.3 Normalized integrated intensities of PL and EL of the two samples as functions of temperature. The injection currents for EL measurements for samples A and B are 1.1 and 1.5 mA, respectively.

Fig. 2.6.4 shows the PL and detection-energy-dependent photoluminescence excitation (DEDPLE) spectra at 10 K of the two samples.

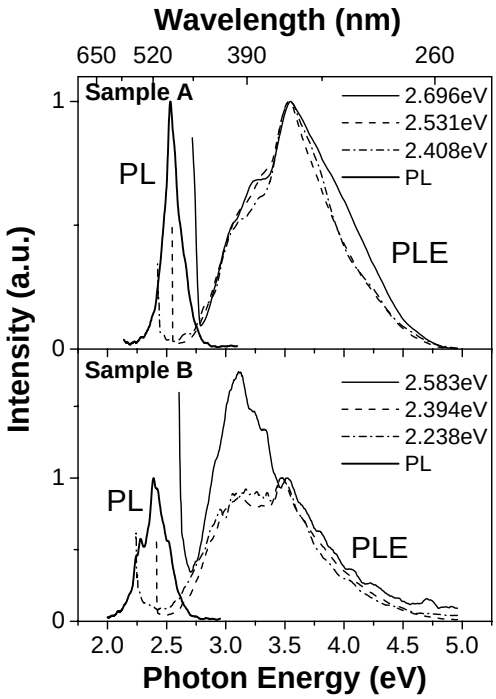

Fig. 2.6.4 DEDPLE and PL spectra of the two samples at 10 K. The PLE spectra are normalized at 3.5 eV, the GaN band gap.

The DEDPLE spectral are normalized at 3.5 eV, which corresponds to the GaN barrier band gap. Compared with sample A, the InGaN absorption features are much stronger, relative to the GaN peak, in sample B. In particular, with a high detection energy level at 2.583 eV, the InGaN absorption is even stronger than GaN in sample B. Such features imply that the QW interfaces in sample B are unclear. In other words, stronger InGaN composition fluctuations exist in sample B. Also, regions of InGaN compositions close to GaN (low indium contents) exist in this sample. The comparison between samples A and B in Fig. 2.6.4 implies that the QW interfacial quality of sample A is higher.

To confirm the quality of QW interface, we performed high-resolution transmission electron microscopy observation. With the two-beam interference data, we could conduct the

SSA for composition distribution images [15]. Figs. 2.5.5 and 2.6.6 show the typical SSA images of samples A and B, respectively. In these SSA images, line scans were conducted along the shown white lines. Here, the line scan values 1 and 1.1, respectively, represent indium compositions of 0 and 60 % (estimated based on the assumption of a specimen thickness larger than 30 nm). Different colors stand for various ranges of indium composition, as shown in the legends.

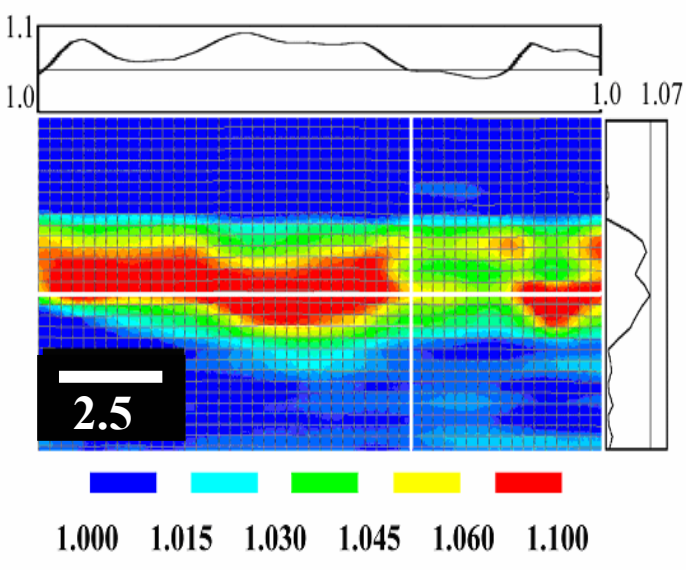

Fig. 2.6.5 A typical strain-state analysis (SSA) image of sample A. The color legend indicates the estimated indium mole fractions (1.0 = 0 %, 1.1 = 60 %).

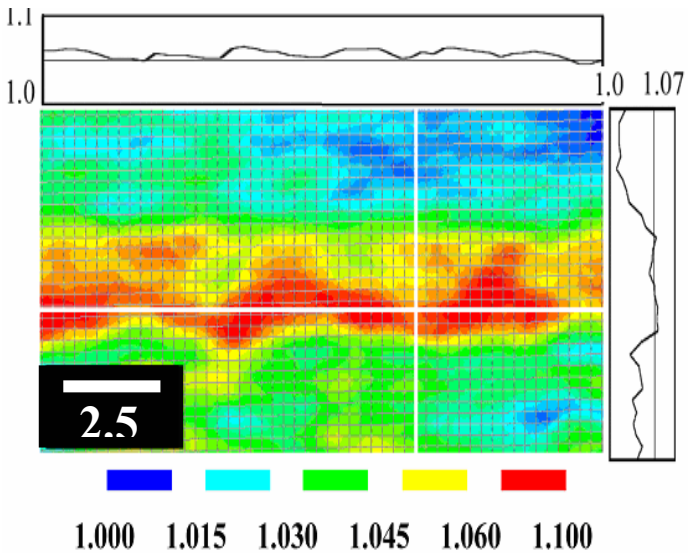

Fig. 2.6.6 A typical strain-state analysis (SSA) image of sample B. The color legend is the same as that in Fig. 2.6.5.

As shown in Fig. 2.6.5, the shape of the QW is quite clear although its thickness is slightly varying. Its boundaries are quite abrupt although indium composition within the well varies in space. In particular, the upper interface in the image is quite clear-cut. Such features can also be clearly seen in the line scan plots. The well defined QW layer in sample A is particularly clear when it is compared with the diffusive nanostructure of sample B, as shown in Fig. 2.6.6. Here, one can see the strongly clustering structure around the designed QW layer although the QW shape is essential recognizable. The strong indium composition fluctuation shown here confirms the strong InGaN absorption features in Fig. 2.6.4. It is believed that the higher QW interface quality shown in Fig. 2.6.5 results in higher photon emission efficiency in sample A,

as indicated in Fig. 2.6.3. It is noted that the two InN interfacial layers cannot be identified in the SSA image of Fig. 2.6.5. This result can be due to the non-existence of such layers in nanostructure. The two InN layers may merge into the QW structure.

2.6.4 Conclusions

In summary, we have compared two InGaN/GaN QW samples in optical property and nanostructure. In one of the samples, InN interfacial layers were placed between wells and barriers for improving the QW interface quality. Compared with the standard barrier-doped QW sample, the addition of the InN interfacial layers did improve the QW interface quality and hence photon emission efficiency. The SSA images showed the high contrast between the clear QW interface in the sample with InN layers and the diffusive QW boundaries in the reference sample. The DEDPLE data revealed the consistent results.

References:

1. K. Watanabe, J. R. Yang, N. Nakanishi, K. Inoke, and M. Shiojiri, Appl. Phys. Lett. **80**, 761 (2002).
2. H. K. Cho, J. Y. Lee, N. Sharma, C. J. Humphreys, G. M. Yang, C. S. Kim, J. H. Song, and P. W. Yu , Appl. Phys. Lett. **81**, 3102 (2002).
3. Y. S. Lin, K. J. Ma, C. Hsu, Y. Y. Chung, C. W. Liu, S. W. Feng, Y. C. Cheng, M. H. Mao, C. C. Yang, H. W. Chuang, C. T. Kuo, J. S. Tsang, and T. E. Weirich, Appl. Phys. Lett. **80**, 2571 (2002).
4. Y. S. Lin, K. J. Ma**,** C. Hsu, S. W. Feng, Y. C. Cheng, C. C. Liao, C. C. Yang, C. C. Chuo, C. M. Lee, and J. I. Chyi, Appl. Phys. Lett. **77**, 2988 (2000).
5. M. Hao, H. Ishikawa, T. Egawa, C. L. Shao, and T. Jimbo, Appl. Phys. Lett. **82**, 4702 (2003).
6. D. I. Florescu, S. M. Ting, J. C. Ramer, D. S. Lee, V. N Merai, A. Parkeh, D. Lu, E. A. Armour, and L. Chernyak, Appl. Phys. Lett. **83**, 33 (2003).
7. S. W. Feng, E. C. Lin, T. Y. Tang, Y. C. Cheng, H. C. Wang, C. C. Yang, K. J. Ma, C. H. Shen, L. C. Chen, K. H. Kim, J. Y. Lin and H. X. Jiang, Appl. Phys. Lett. **83**, 3906 (2003).
8. Y. C. Cheng, C. H. Tseng, C. Hsu, K. J. Ma, S. W. Feng, E. C. Lin, C. C. Yang, and J. I. Chyi, IEEE J. Electronic Materials, **32**, 375 (2003).
9. S. Chichibu, K. Wada, and S. Nakamura, Appl. Phys. Lett. **71**, 2346 (1997).
10. Y. S. Lin, C. C. Yan, C. Hsu, K. J. Ma, Y. Y. Chung, S. W. Feng, Y. C. Cheng, E. C. Lin, C. C. Yang, C. T Kuo, and J. S. Tsang, J. Crystal Growth, **252**, 107 (2003).
11. C. M. Lee, C. C. Chuo, J. F. Dai, X. F. Zheng, and J. I. Chyi, J. Appl. Phys. **89**, 6554 (2001).
12. X. A. Cao, S. F. LeBoeuf, L. B. Rowland, C. H. Yan, and H. Liu, Appl. Phys. Lett. **82**, 3614 (2003).
13. C. C. Liao, S. W. Feng, C. C. Yang, Y. S. Lin**,** K. J. Ma**,** C. C. Chuo, C. M. Lee, and J. I. Chyi, Appl. Phys. Lett.. **76**, 318 (2000).
14. T. J. Schmidt, Y. H. Cho, G. H. Gainer, J. J. Song, S. Keller, U. K. Mishra, and S. P. DenBaars, Appl. Phys. Lett. **73**, 560 (1998).
15. D. Gerthsen, B. Neubauer, A. Rosenauer, T. Stephan, H. Kalt, O. Schon and M. Heuken, Appl. Phys. Lett. **69**, 2701 (1996).

CONCLUSIONS

The performed optical and microstructure analysis evidences on an improvement of the MQW structural quality and increased emission efficiency in the thicker structures upon post growth thermal annealing. Differences in degree of disorder in as-grown samples of various well width leads to different impact of thermal annealing on luminescence from localized states. The blue shift of the PL peak and pronounced changes in the absorbance indicate a remarkable interdiffusion of indium at the quantum well barrier interface for thin MQWs. While the pronounced red shift in PL and an increase in the excitation lifetime in thicker MQWs is attributed to manifestation of the QCSE due to built-in field. Also, MWQs of larger thickness were shown to possess larger variations in potential profile and a larger amount of structural defects.

A comparison of experimentally obtained redshift of PL band with calculated energy of the lowest optical transition in InGaN MQW enables partial separation of contributions of the well tilting due to the quantum-confined Stark effect and the carrier localization that affect carriers accumulated in In-rich regions. The increasing carrier generation rate causes filling of the localized states (with typical average localization energy of ~30-40 meV in $In_{0.15}Ga_{0.85}N$). The further increase of excitation intensity causes screening of the built-in electric field and, hence, the further blueshift of the PL band. The screening effect is stronger and, hence, the carrier density is higher when PL of the same intensity is excited via generation of carriers into the barrier layers as compared with selective excitation of the wells. This result is in consistence with existence of In-rich regions, which are formed at the well-barrier interface and extend into the barrier.

We have demonstrated an analysis of temperature behavior of the PL line width in InGaN/GaN MQWs by using Monte Carlo simulation of exciton hopping. The simulation revealed band potential fluctuations within individual In-rich regions (31 meV), dispersion of the average exciton energy in different In-rich regions (29 meV), and a Bose-Einstein-like temperature dependence of the average exciton energy in the wells. The localized-state energy dispersion σ for hopping of excitons within isolated In-rich regions increase with increasing In content from 31 eV in the sample with the lowest In content to 38 meV in sample with the highest In content. Meanwhile, the dispersion Γ due to different average indium content within the In-rich regions changes from 29 to 47 meV in the same samples, respectively. Our results suggest that excitons migrate and radiatively recombine within isolated In-rich regions with the average band potential lower than that in the surrounding InGaN matrix. Increased In molar fraction results mainly in an increase in dispersion of the average energy of In-rich regions, meanwhile the band potential fluctuations within the regions increase to a smaller extent.

We have installed and approved the deep level transient spectroscopy (DLTS) for investigation of trapping states in GaN muli quantum well structures. In order to assess the usability of DLTS technique for study the deep trapping levels in multi-quantum well structures both the thermostimulated depolarization (TSD), thermostimulated capacitance relaxation (TSC) and DLTS are studied in p-n homojunction GaN diode structure for the first time. It is shown that cooling of the GaInN MQW structure down to liquid helium temperatures results in complete trapping both the majority and the minority charge carriers at the shallow dopand levels. It is shown that using DLTS technique it is possible to obtain the thermal ionization energies of deep electron states in the MQW structures. Thus, the DLTS technique extended wit DSD and TSC measurements is suitable for investigation of deep trapping states in MQW structures.

We have started the *ab initio* calculations of the neutral and charged defects in GaN. Formation of localized electronic states followed by localization of excess charge carriers has

been considered. Impurities of Mg, Zn, Li, Si and C atoms (the most common dopants) and vacancies of Ga and N are examined. We are started calculations of the electronic states of In in GaN as the homovalent impurity with the aim investigation of the clasterization effects to draw conclusions about role of In aggregates in electronic processes in MQW structures.

We have compared the results of site selective photoluminescence techniques and strain state analysis images of InGaN/GaN QW samples with un-doped, well-doped, and barrier-doped structures. The strain state analysis images showed strongly clustering nanostructures in the barrier-doped sample and relatively weaker composition fluctuations in the undoped and well-doped samples. Such variations in nanostructure resulted in different carrier transport processes. Also, the PL results provided us clues for speculating that the S-shape PL peak position behavior is dominated by the QCSE in an undoped InGaN/GaN QW structure. However, carrier localization is more effective in blue-shifting luminescence and improving radiative efficiency of a sample, when compared with the relaxation of QCSE. It was shown that the addition of the InN interfacial layers did improve the QW interface quality and hence photon emission efficiency.

Further study of the impact of Si doping on carrier localization are foreseen by combing the expertise and the spectroscopy methods combined with theoretical modeling of carrier migration and QCSE in InGaN/GaN MQWs.